A rapid transfer of virions coated with heparan sulfate from the ECM to CD151 defines an early step in the human papillomavirus infection cascade

Annika Massenberg[1], Yahya Homsi[1], Carl Niklas Schneider[1], Snježana Mikuličić[2], Tatjana Döring[2], Luise Florin[2,3,*], Thorsten Lang[1,*]

[1]University of Bonn, Faculty of Mathematics and Natural Sciences, Membrane Biochemistry, Life & Medical Sciences (LIMES) Institute, Carl-Troll-Straße 31, 53115 Bonn, Germany
[2]Institute for Virology, University Medical Center of the Johannes Gutenberg-University Mainz, Obere Zahlbacher Straße 67, 55131 Mainz, Germany
[3] Research Center for Immunotherapy (FZI), University Medical Center of the Johannes Gutenberg-University Mainz, 55131 Mainz, Germany

*Correspondence should be addressed to Thorsten Lang (thorsten.lang@uni-bonn.de) or Luise Florin (lflorin@uni-mainz.de)

Keywords: virus infection, primary attachment site, secondary receptor, filopodia, transport, tetraspanins

Abstract

Human Papillomaviruses (HPVs) are the underlying cause of several types of cancer, albeit they are mostly known for their association with cervical carcinoma. The virions must reach their target cells through a break in the epithelial barrier. After binding to heparan sulfate (HS) of the extracellular matrix (ECM), they translocate to the cell surface and co-internalize with the entry factor CD151.

The *in vivo* occurring translocation from the ECM to entry factors at the cell membrane may be bypassed in nonpolarized cells with low ECM secretion. To specifically investigate these early events of the infection cascade, we use polarized keratinocytes. They produce a robust ECM and have a restricted expression of entry receptors primarily to the substrate-adhered basal membrane. Virion access to the basal membrane by diffusion is strongly limited, such that translocation from the ECM is the main pathway used for infection. We block the translocation from ECM attachment sites to the cell body, release the blocking, and monitor the association of virions with CD151 or HS. We observe quick virion translocation from the ECM to the cell body within 15 min. During translocation, virions associate with the tetraspanin CD151 present at the cell border or at filopodia. Translocating virions are decorated with HS, which they lose in the next few hours, presumably prior to endocytosis.

37 Our observations reveal a rapid step in the HPV infection cascade: the transfer of HS-coated
38 virions from the ECM to CD151. This step is too fast to account for the asynchronous uptake of HPVs
39 which is likely driven by glycan- and capsid processing.
40
41
42 **Introduction**
43 Already in the 80s, Harald zur Hausen proposed a role of human papillomaviruses in cancer
44 (***zur Hausen, 2009***). Since then, five more classes of oncogenic viruses have been identified (***Galati et***
45 ***al., 2024a***). To date, it is assumed that more than 10% of the worldwide human cancer burden is
46 associated with infectious agents (***Galati et al., 2024a***), from which about a half is caused by
47 *Papillomaviridae* (***Martel et al., 2017***). Thus, the understanding of viral entry strategies has
48 implications going beyond the classical treatment of acute viral infections.
49 Human papillomaviruses are small, non-enveloped viruses with a diameter of ≈55 nm. The
50 icosahedral capsid is mainly composed of pentameric L1 capsomers. Together with less L2 capsid
51 proteins, capsomers surround a histone core bearing a circular double-stranded DNA (***Baker et al.,***
52 ***1991; Ozbun and Campos, 2021***). From the more than 200 phylogenetically classified HPV genotypes,
53 the most oncogenic ones are HPV16 and HPV18 (***Galati et al., 2024b***), which are responsible for about
54 70 - 80% of the cervical cancer cases (***Christiansen et al., 2015***). In addition, they cause other severe
55 cancers such as anogenital, head and neck tumors (***Doorbar et al., 2012***).
56 For papillomavirus infection, a disruption of the epithelial barrier is a prerequisite, through
57 which virions reach mitotically active basal cells of the epithelia (***Ozbun, 2019***). Here, virions bind to
58 the linear polysaccharide heparan sulfate (HS) that is present in the extracellular matrix (ECM) but as
59 well on the plasma membrane surface. HS is attached to proteins forming so called heparan sulfate
60 proteoglycans (HSPGs). Positively charged and polar residues of the L1 capsid protein form multiple
61 heparan sulfate binding sites that interact with negative charges of HS, resulting in a strong bond and
62 virus uptake into the infectious pathway (***Dasgupta et al., 2011; Giroglou et al., 2001; Joyce et al.,***
63 ***1999; Knappe et al., 2007; Surviladze et al., 2015***). While in cell culture virions bind to HS on both the
64 cell surface and the ECM, it has been suggested that *in vivo* they bind predominantly to HS of the
65 extracellular basement membrane (***Day and Schelhaas, 2014; Kines et al., 2009; Ozbun and Campos,***
66 ***2021; Schiller et al., 2010***). In any case, the tight bond between the linear polysaccharide and virions
67 must be disrupted before they can bind to a yet unknown secondary receptor on the cell surface,
68 followed by internalization (***Ozbun and Campos, 2021***).
69 The strong electrostatic bonding precludes HS release via dissociation. Two release
70 mechanisms are discussed, that mutually are not exclusive. In the so-called priming model, binding to

71 HS structurally results in capsid enlargement and softening (***Feng et al., 2024***), followed by the
72 exposure and cleavage of L1 by kallikrein-8 (KLK8) (***Cerqueira et al., 2015***), exposure of L2 by
73 cyclophilin (***Bienkowska-Haba et al., 2009***), and L2 cleavage by furin (***Richards et al., 2006***). After
74 these structural modifications of the capsid surface the 'primed' virion is able to bind to the secondary
75 receptor. In an alternative model, the HS-virion bond remains. However, cleavage of HS/HSPGs by
76 heparanases and proteinases produces HS fragments. Therefore, albeit still bound to the virion
77 surface, the fragmented HS no longer anchors the virion to the ECM (***Surviladze et al., 2012;***
78 ***Surviladze et al., 2015***).
79 Once the virions are released, they could reach the cell surface simply by passive diffusion. In
80 a co-culture trans-well assay, pseudovirions (PsVs) from donor cells infect spatially separated receiver
81 cells (***Surviladze et al., 2012***), demonstrating that free diffusion of virions may be sufficient for
82 infection. However, an active transport mechanism has been reported as well. PsVs migrate along
83 actin-rich protrusions from the ECM towards the cell body (***Schelhaas et al., 2008; Smith et al., 2008***).
84 While it is generally agreed on that HS is a primary virion attachment site, the molecular
85 identity of the secondary receptor on the main cell body surface is unknown. The secondary complex
86 is most likely a multimeric complex rather than a single molecular component. Possible candidates are
87 proteins crucial for cell entry, as the tetraspanin CD151 (***Mikuličić et al., 2019; Scheffer et al., 2013;***
88 ***Spoden et al., 2008***), integrin-α6 (Itgα6) (***Evander et al., 1997; Yoon et al., 2001***), growth factor
89 receptors (***Mikuličić et al., 2019; Surviladze et al., 2012***), and the annexin A2 heterotetramer
90 (***Dziduszko and Ozbun, 2013; Woodham et al., 2012***). From these molecules, the tetraspanin CD151
91 could play a coordinating role, as tetraspanins organize viral entry platforms in many types of viral
92 infections, including infections with coronavirus, cytomegalovirus, hepatitis C virus, human
93 immunodeficiency virus, human papilloma virus, and influenza virus (***Bruening et al., 2018; Earnest et***
94 ***al., 2015; Florin and Lang, 2018; Hantak et al., 2019; Hochdorfer et al., 2016; Scheffer et al., 2013;***
95 ***Zona et al., 2013***). Tetraspanin entry platforms could form in a slow and stochastic fashion, which
96 would provide an explanation for the asynchronous virion uptake with half-times of above 10 h
97 (***Becker et al., 2018***). However, it is unclear whether virions associate with CD151 already in the
98 moment of virion transfer from the ECM to the cell surface or afterwards in preparation of the
99 endocytic uptake.
100 In this study, we explore the relationship between actin-dependent transport and CD151
101 association in HPV infection. We employ the cell permeable mycotoxin and actin polymerization
102 inhibitor cytochalasin D (CytD). We find that CytD causes the trapping of HPV16 PsVs in the ECM of a
103 polarized human keratinocyte cell line (HaCaT cells), where they remain accumulated adjacent to the
104 cell periphery. This blocking of the virus transfer is accompanied by co-accumulation of HS in the ECM

105 area. Upon CytD removal, HS-decorated PsVs move from the ECM to the cell body and CD151. The
106 association of PsVs with CD151 persists within the next few hours, whereas the HS coat is stripped off.
107 These findings distinguish a step in the infection cascade with CD151 playing an early role directly after
108 the release of virions from the ECM.
109
110
111 **Results**
112 *Cytochalasin D arrests the translocation of HPV16 PsVs from the extracellular matrix to the cell body*
113 *surface*
114 The molecular surface of PsVs is immunologically indistinguishable from HPV virus particles
115 (***Ozbun and Campos, 2021***), which makes them a widely used tool for studying host cell entry. In this
116 study, we employ HPV16 pseudovirions with an encapsidated luciferase reporter plasmid under the
117 control of the HPV16 promotor (***Wüstenhagen et al., 2018***). Hence, instead of viral DNA a luciferase
118 encoding plasmid enters the nucleus, enabling the analysis of the infection rate via the luciferase
119 activity. Moreover, the plasmids are composed of nucleotides to which fluorophores can be coupled
120 by click-chemistry. This allows for their detection by fluorescence microscopy throughout the entire
121 infection pathway.
122 Many PsVs that bind to the ECM may locate distal from the cell surface and are thus unable
123 to establish direct contact with entry receptors. However, they are capable of migrating by an actin-
124 dependent transport along cell protrusions towards the cell body (***Schelhaas et al., 2008; Smith et al.,***
125 ***2008***). We aimed for blocking this transport in HaCaT cells, a cell line that is widely used as a cell culture
126 model for HPV infection. HaCaT cells closely resemble primary keratinocytes in key aspects: they are
127 not virally transformed and produce large amounts of ECM that facilitates infection (***Bienkowska-***
128 ***Haba et al., 2018; Gilson et al., 2020***). In addition, HaCaT cells exhibit cellular polarity that enforces
129 binding of virus particles to the ECM, as the virions cannot bind to receptors/entry components, such
130 as CD151, Itgα6 and HSPGs that co-distribute on the basolateral membrane of polarized keratinocytes
131 (***Cowin et al., 2006; Mertens et al., 1996; Sterk et al., 2000***), making them inaccessible by diffusion.
132 We incubate cells for 5 h with PsVs in the absence or presence of 10 µg/ml CytD. Previously,
133 it has been shown that this CytD concentration stops cell migration after a few minutes (***Peng et al.,***
134 ***2011***). Frequently, we observe patches of confluent cells which are common to HaCaT cells. Cells at
135 the center of these patches are dismissed during imaging, because there are no anterogradely
136 migrating PsVs at these cells. A second reason for our dismissal of these cells is that hardly any PsVs
137 are bound to them, possibly because their basal membranes are inaccessible by diffusion. Instead, we
138 focus on isolated HaCaT cells or cells at the periphery of cell patches. At these cells, we find more PsVs
139 per cell than one would expect from the employed 50 viral genome equivalents (vge) per cell,

140 indicating that PsVs are unequally distributed between the cells. Moreover, these PsVs usually are not
141 homogenously distributed around the cell but concentrate at one region. We investigate the
142 translocation of PsVs from these regions, defining ROIs for analysis that cover PsVs at the periphery
143 and the cell body (see Supplementary Figures 6A and 8A). After the 5 h incubation, cells were fixed
144 and stained by a membrane marker, the dye TMA-DPH, to mark the main cell body (Figure 1A, gray
145 lookup table (LUT)). Additionally, they were stained for PsVs (by click-chemistry; magenta LUT), HS
146 (antibody staining; cyan LUT), and the membrane protein Itgα6 (antibody staining; green LUT). In the
147 control, PsVs locate mostly in the cell body area (Figure 1A, upper row; see white outline that is based
148 on TMA-DPH staining). In contrast, when CytD was present, the cell body area is largely devoid of PsVs
149 (Figure 1A, lower row; please note that the large central bright area is mainly caused by
150 autofluorescence). Instead, PsVs often accumulate adjacent to the cell body. This adjacent region that
151 is up to several µm wide and rich in HS, likely contains the ECM. We conclude that, upon inhibition of
152 actin-dynamics by CytD, PsVs remain accumulated in the ECM area.

153 Comparing in Figure 1A the PsV brightness in the upper (control, magenta LUT) and lower
154 (CytD, magenta LUT) panels suggests that the amount of PsVs does not differ greatly. This is surprising,
155 as CytD is not reported to inhibit enzymes involved in capsid modification or HS/HSPGs processing,
156 after which the PsVs supposedly leave the ECM. If this were the case, one would expect no difference
157 in the number of PsVs at the periphery between cells that were treated with or without CytD for 5 h.
158 Therefore, we conclude that PsVs remain ECM associated while ready for binding to a secondary
159 receptor. However, a quantification of the PsVs with and without CytD is not possible in this
160 experiment, due to interference from autofluorescence (Figure 1A, large magenta area in the center).
161 To study PsVs in the absence of autofluorescence, we employed unroofed cells (***Heuser, 2000***), also
162 referred to as membrane sheets. After pre-treatment of cells as above, membrane sheets are
163 generated by brief ultrasound pulses that remove the upper cellular parts (and thus any intracellular
164 autofluorescence), leaving behind the extracellular matrix and the basal membrane along with the
165 bound PsVs. During imaging, membrane sheets are identified via staining of F-actin with fluorescently
166 labelled phalloidin (Figure 1B, green LUT) that marks the main cell body cortex together with
167 lamellipodia and filopodia. In this experiment we observe that PsVs, not always but frequently,
168 accumulate adjacent to the isolated basal membrane (defined by F-actin staining, Figure 1B, green
169 LUT) after CytD treatment, which differs from the control (Figure 1B, magenta LUT).

170 The PsV maxima density (Figure 1B, magenta LUT, detected as local maxima of antibody
171 stained L1) and the PsV intensity are quantified in an area covering the cell body and the periphery.
172 Compared to the control, CytD reduces the PsV maxima density by 26% (the PsV maxima density in
173 the control and CytD treated cells is 0.7 and 0.52 PsVs/µm^2, respectively), whereas the maxima

174 intensity increases by 41% (Figure 1C). A histogram of the PsV maxima intensities illustrates that CytD
175 broadens the intensity distribution towards brighter PsVs (Figure 1D). The increase of the PsV intensity
176 after CytD treatment can also be appreciated comparing the upper and middle/lower L1 image of
177 Figure 1B (shown at the same settings of brightness and contrast). As CytD is unlikely to act directly
178 on PsVs (e.g., by fusing them to larger and brighter particles), we assume that the underlying cause of
179 brighter maxima is the resolution limit of the microscope. The densely accumulated PsVs are no longer
180 resolved and merge to brighter spots. These poorly resolved maxima are on average 41% brighter but
181 of them there are 26% fewer. The decrease in maxima density is in the order of magnitude of the
182 increase in intensity, which yields a roughly similar total signal in both conditions.

183 We addressed whether PsVs would still be accumulated when adding CytD 1 h after the PsVs
184 rather than simultaneously (Figure 1B, lower panel, CytD after 1 h). As in the CytD condition, we
185 frequently see accumulated PsVs adjacent to the isolated basal membrane (Figure 1B, arrows point
186 towards PsV accumulations). The PsV maxima intensity distribution is broader when compared to the
187 control but narrower than with CytD present the entire time (Figure 1D). We conclude that complete
188 PsV binding and translocation takes longer than 1 h, as otherwise control and CytD after 1 h should be
189 more similar.

190 At this point, one could conclude from the data that CytD arrests PsVs on their journey
191 towards the cell body and that PsVs are not collected from the cells, but remain trapped in the ECM.
192 How efficient PsV trapping is cannot be determined exactly for several reasons. First, our assay is not
193 precise for technical reasons, as the above-mentioned limited resolution results in an underestimation
194 of the number of PsVs the stronger they are accumulated. Second, we do not know how many PsVs in
195 the control become endocytosed during the 5 h of incubation. This reduces the PsVs in the control,
196 which is our value for comparison. Moreover, it should be noted that both the degree of PsV
197 accumulation as well as the number of PsVs are highly variable. Even in the absence of CytD, we
198 occasionally find cells with accumulated PsVs at the periphery, whereas such cells are more frequently
199 observed after CytD. This causes a large variability within the data. Still, we consider larger PsV
200 accumulations after CytD as a typical effect (please note that for illustration of this effect we show in
201 the Figures such examples). Despite these limitations, it appears that within the 5 h incubation period
202 with CytD a large fraction of PsVs remains associated with the ECM.

203 During the CytD incubation, PsVs bind to HSPGs of the basolateral membrane for 5 h. Still, in
204 the cell body area hardly any PsVs are present (0.14 PsV/μm^2, Supplementary Figure 1B). In the
205 control, the PsV density is several-fold larger (Supplementary Figure 1B). This is expected, as the PsVs
206 bind to the ECM and translocate to the cell body. We wondered whether there are more binding sites
207 at the basal membrane that, however, remain inaccessible to PsVs by diffusion, because of the

208 insufficient space between glass-coverslip and basolateral membrane. For clarification, we incubated
209 EDTA detached HaCaT cells in suspension with PsVs for 1 h at 4 °C, followed by re-attachment for 1 h.
210 Under these conditions, we find a PsV density 12.4-fold larger than after 5 h of CytD incubation of
211 adhered cells (Supplementary Figure 1B and D). However, it should be noted that these values cannot
212 be directly compared. Aside from the different treatments, another difference lies in the size of the
213 basal membrane, as re-attachment of cells is not complete after only 1 h (compare size of adhered
214 membranes in Supplementary Figure 1A and C). Therefore, the imaged membranes are likely strongly
215 ruffled, which results in the underestimation of the size of the adhered membrane. As a result, we
216 overestimate the PsVs per μm^2 (please note that we cannot re-attach cells for longer times as we
217 would then lose PsVs due to endocytosis). On the other hand, we would underestimate the PsV density
218 at the basal membrane if after re-attachment we image in part also some apical membrane. In any
219 case, the experiment suggests that PsVs bind more efficiently if membrane surface receptors are
220 accessible by diffusion. This is in support of the above notion that the basal membrane may provide
221 more entry receptors than one would expect from the low density of PsVs bound after 5 h CytD
222 (Supplementary Figure 1B). This suggests that under our assay conditions, PsVs cannot easily bypass
223 the translocation from the ECM to the cell body by diffusing directly to the basal membrane. Hence,
224 the large majority of PsVs that enter the cell were previously bound to the ECM. Therefore, HaCaT
225 cells serve as an ideal model for studying the transfer of ECM bound HPV particles to the cell surface,
226 which is similar to *in vivo* infection of basal keratinocytes after binding to the basement membrane
227 (***Bienkowska-Haba et al., 2018; Day and Schelhaas, 2014; Kines et al., 2009; Schiller et al., 2010***).
228
229 *The blocking of PsV translocation by cytochalasin D is reversible*
230 CytD not only arrests the transport of PsVs to the cell but is known to block other actin-
231 dependent processes, which strongly affects the physiology of the cell. Therefore, we investigated
232 whether PsVs would proceed normally on their infection pathway once CytD is washed off. In order
233 to allow for recovery from CytD, cells were washed after the 5 h simultaneous PsV/CytD treatment,
234 then incubated for another 19 h and the infection rate was subsequently determined by measuring
235 the luciferase activity in the cell lysate. CytD reduced luciferase activity by 29%, as compared to the
236 control (Figure 1E; left). A certain degree of reduced infectivity is to be expected, as PsVs have ≈20%
237 less time to complete infection as compared to cells that were not treated with CytD. When PsVs were
238 not washed off after 5 h but left for the entire 24 h incubation, the infection rate increased by 52%,
239 whereas continuous treatment with CytD results in no infection (Figure 1E; right). The latter is in line
240 with previous studies (***Schelhaas et al., 2008; Selinka et al., 2002; Selinka et al., 2007; Spoden et al.,***
241 ***2013***) showing that CytD is a strong inhibitor of HPV infection. In any case, PsVs proceed on the

242 infection pathway upon removal of CytD. The reduced infection rate of 29% can be explained by the
243 5 h blocking at the beginning of the incubation period that should delay the time course of infection.
244 Therefore, we propose that CytD is suitable for transiently arresting PsVs in a state between primary
245 attachment to HS and cell body secondary receptor binding.

246 Next, we investigated the onset of PsV translocation after CytD wash off. Cells were treated
247 with PsVs and CytD for 5 h, washed, and incubated further without PsVs/CytD for 0 min, 30 min or
248 60 min, followed by fixation and staining for PsVs (Figure 2A, magenta LUT) and F-actin (Figure 2A,
249 green LUT). The antibody staining against PsVs, like above the click-chemistry staining, is again highly
250 variable. For analyzing the translocation process, we calculated the Pearson correlation coefficient
251 (PCC) between PsV-L1 and F-actin staining. The PCC quantifies the similarity between two variables,
252 in this case the pixel values of the two images. The PCC results in the value of 1 if images overlap
253 perfectly and -1 for an image and its negative. After 5 h of CytD, PsVs again accumulate at the edge of
254 the F-actin staining (Figure 2A, compare to Figure 1B that shows membrane sheets). The distal PsVs
255 and the F-actin staining partially exclude each other, thus at 0 min we obtain a negative PCC (Figure
256 2A and D). After 30 min and 60 min, PsVs mostly overlap with F-actin stained areas, which results in
257 positive PCCs (Figure 2A and D). The time course of the change in PCC values suggests an onset of
258 translocation recovery within 30 min after CytD removal.

259

260 *Assessing previously proposed steps in HPV infection in our assay*

261 PsVs reportedly bind tightly to their primary attachment site until the capsid surface
262 undergoes structural changes, which involves modifications of L1 and L2 (see above). Consequently,
263 we would expect that inhibition of L1 processing during the CytD incubation prevents the recovery of
264 PsV translocation from the ECM to the cell body (Figure 2A and D). To test for this possibility, as
265 employed in earlier studies, the protease inhibitor leupeptin was used to inhibit proteases including
266 KLK8 which is required for L1 cleavage (***Cerqueira et al., 2015***). Employing this inhibitor, the PCC
267 between PsV-L1 and F-actin staining remains negative after CytD removal, showing that for
268 translocation indeed the action of proteases is required (Figure 2B and D). In contrast, inhibition of L2
269 cleavage by a furin specific inhibitor has no effect on the PCC (Figure 2C and D). However, it should be
270 noted that we occasionally observe PsVs not completely translocating but accumulating at the border
271 of the F-actin stained area (for example see Figure 2C (60 min)). This results in an increase of the PCC
272 almost equal to complete translocation, explaining why the PCC remains unaffected despite a furin
273 inhibitory effect. Hence, furin inhibition may have some effect on translocation that, however, is
274 undetected in this type of analysis.

275 As outlined above, during the 5 h incubation with CytD, proteases in the ECM are expected to
276 cleave HS chains. These cleavage products should be able to diffuse out of the ECM, unless they remain
277 associated with non-translocating PsVs. On the other hand, in the control, less HS cleavage products
278 are trapped and if trapped the PsV leave the ECM. So far, and throughout the entire study, we stain
279 the cells without prior cell permeabilization (albeit fixation perforates the cell membrane to some
280 extent) in order to monitor only cell surface events. Using an antibody that reacts with an epitope in
281 native heparan sulfate chains, only after CytD and if PsVs were present, the level of HS staining was
282 significantly increased (Figure 3B). As shown in Figure 3A, stronger HS staining at PsVs (open arrows)
283 and as well in PsV free areas (closed arrows) was observed.
284 As additional control and shown in Supplementary Figure 2, we used an antibody that reacts
285 with a HS neo-epitope generated by heparitinase-treated heparan sulfate chains (***Yokoyama et al.,***
286 ***1999***; for details see methods). This neo-epitope staining is independent of the presence of CytD and
287 the incubation time, suggesting that CytD does not directly affect HS processing. Collectively, our
288 findings indicate that without actin-dependent PsV translocation HS cleavage products are retained in
289 the ECM, consistent with the hypothesis that cleaved HS remains associated with PsVs (***Ozbun and***
290 ***Campos, 2021***).
291
292 *The transfer of PsVs from the ECM to the cell body is fast and efficient*
293 Next, we studied the time course of PsV translocation in more detail. Cells were treated as in
294 Figure 1A (in Figure 4, the 0 min time point is identical), followed by removal of PsVs/CytD. Different
295 from Figure 2, we did not calculate the PCC that provides only an approximate idea of the time course
296 of translocation, but monitored the diminishment of the integrated density of PsVs locating at the cell
297 periphery after 0, 15, 30 and 60 min. The cell periphery is delineated from the cell body by the TMA-
298 DPH membrane staining (Figure 4A, the cell periphery is defined by the area enclosed by the two white
299 lines in the images shown with the magenta LUT).
300 At 0 min, compared to the control, CytD causes a 6-fold increase of PsV signal in the periphery
301 (Figure 4B). This increase is more than halved when cells were incubated for 15 min, and after 30 min,
302 the level of the control is reached (Figure 4B). This suggests that the half-time of PsV translocation
303 from the periphery to the cell body is about 15 min. In fact, the half-time maybe longer, as we cannot
304 exclude that cell spreading after CytD removal contributes to less PsVs measured in the cell periphery.
305 In any case, translocation is fast and efficient and not a major component in the time course of
306 infection. We conclude that translocation is not responsible for the asynchronous virion uptake
307 observed for HPV PsVs.
308
309 *Translocation of PsVs to CD151*

310 During translocation, at some point PsVs may approach to cell surface HPV entry factors, like
311 the tetraspanin CD151. For studying this possibility, we employ superresolution STED microscopy,
312 analyzing the association of PsVs with CD151 over time. Cells are treated and monitored as above, but
313 with an extended time window of up to 180 min, as cell surface processes are expected to take longer
314 than an hour.

315 After fixation, PsVs and CD151 were double-stained with antibodies against L1 (Figure 5A,
316 magenta LUT) and CD151 (Figure 5A, green LUT). In addition, we stained F-actin with fluorescent
317 labelled phalloidin. We simultaneously image L1 and F-actin in the confocal and CD151 in the STED
318 channel.

319 As shown in Figure 5A, CD151 concentrates in spots scattered across the cell surface. It is also
320 present at cell protrusions that are rich in F-actin and vary strongly in number and shape
321 (Supplementary Figure 3A shows some examples of these filopodia). Compared to the control, CytD
322 again preserves the accumulated PsVs at the cell periphery, and at early time points PsVs appear
323 brighter (Figure 5A; for overview images and F-actin staining see Supplementary Figure 4A and B; for
324 variability of PsV accumulations after CytD see Supplementary Figure 4B).

325 Initially, we wondered whether, after reaching the cell body, PsVs are transported quickly
326 further towards the center of the cell body. Based on the CD151 image, a cell border region was
327 defined (for details see Supplementary Figure 3B). We counted the number of PsVs in this region, and
328 expressed it as percentage of all PsVs in the image. In the control, the fraction of PsVs in the cell border
329 region was rather low, ranging from 13.4% (0 min) to 7.6% (180 min). After CytD, at 0 min, compared
330 to the control the fraction almost tripled (36.5%). It diminished to 16.9% after 60 min, and 12.3% after
331 180 min (Supplementary Figure 3C). This suggests that PsVs only briefly remain in the cell periphery.

332 The intensity of the CD151 staining between cells is highly variable (Figure 5A and B). In the
333 control, the mean CD151 intensity shows no trend over the 180 min time course, whereas with CytD
334 the intensity diminishes after 180 min (Figure 5B). The decrease of the CD151 staining intensity points
335 towards the possibility that, after CytD wash off, CD151 is more strongly internalized, presumably due
336 to co-internalization with endocytosed PsVs. This idea is supported by the observation that, in
337 particular at CytD/180 min, we occasionally observe CD151/PsV agglomerations (Figure 5A, see
338 structures marked by arrows at CytD/180 min, for more examples see Supplementary Figure 5A). We
339 did not study this issue systematically, but some of these structures have clear three-dimensional
340 extension (see Supplementary Figure 5B for axial scans). Therefore, they are likely tubular structures
341 filled with several PsVs, as previously described by electron microscopy (***Schelhaas et al., 2012***). We
342 observe fewer of such structures at control/180 min, probably because cells have been actively
343 interacting with PsVs for altogether 8 h, opposed to 3 h in the CytD treated cells. Hence, in the control,

344 PsV endocytosis may be less synchronized compared to CytD explaining the CD151 diminishment at
345 CytD/180 min (Figure 5B).
346 For studying the association between PsVs (L1) and CD151, the PCC between the channels is
347 calculated. The PCCs are around 0.1, with the exception of the CytD/0 min value that is significantly
348 lower and even negative (Figure 5C, for PCC values of flipped images see Supplementary Figure 6).
349 This reflects the somewhat mutual exclusion of the two stainings as already discussed above; PsV
350 accumulations are at the cell periphery and the CD151 staining is mainly at the cell body and in
351 filopodia. At 30 min after CytD, the PCC has reached the level of 0.1 as in the other conditions,
352 suggesting that actin processes are required early for the PsV-CD151 association.
353 One would expect that the translocation of PsVs to the cell surface increases the number of
354 PsVs that are closely associated with CD151. As criteria for close association, we define a distance of
355 ≤ 80 nm between PsV and CD151 maxima, a value which is close to the resolution limit of the used
356 microscope (***Finke et al., 2020***). In the control, the fraction of PsVs closely associated with CD151, after
357 correction for random background association (see Supplementary Figure 7), is 8.7% (Figure 5D,
358 control). At 0 min after CytD, we start with a fraction of 5.5%, a value that increases to 12.7% in the
359 next 60 min (CytD/60 min), although this change is not significant (Figure 5D, CytD).
360 Altogether, we conclude that after a 5 h pre-incubation with PsVs (Figure 5D, control), about
361 10% of the PsVs are associated closely with CD151 in a time window of 180 min. CytD diminishes only
362 the early association at 0 min (5.5%, Figure 5D, CytD). The data suggests that PsVs establish contact to
363 CD151 assemblies early in the infection cascade (see also the increase in the PCC after CytD between
364 0 and 30 min, Figure 5C).
365
366 *PsV association with HS*
367 Next, we studied the association between PsVs and HS. As a reference staining for the cell
368 body, we used Itgα6 that is not visible at cell protrusions. PsVs are visualized by click-chemistry and
369 imaged in the confocal channel. HS and Itgα6 were stained by antibodies, and imaged at STED
370 microscopic resolution. The three stainings were simultaneously recorded.
371 As shown in Figure 6A (green LUT), the Itgα6 staining results in a pattern of dense spots. The
372 Itgα6 intensity does not change over time (Supplementary Figure 8E). The pattern of the HS staining
373 (cyan LUT) and the overlap of HS with PsVs and Itgα6 are highly variable (Figure 6A).
374 CytD increases the intensity of HS (Figure 6B; also apparent when comparing the HS brightness
375 in the upper and lower panels of Figure 6A; for an overview of the CytD/0min images see
376 Supplementary Figure 4C). This increase of intensity is particularly notable at the 0 min time point,
377 where the samples treated with CytD have a more than two-fold higher intensity and differ

378 significantly from the control. Hence, in this experiment we reproduce the PsV/CytD mediated HS
379 intensity increase observed in Figure 3.

380 In the control, the PCC between PsVs and HS is little above zero. The largest PCC is found at
381 CytD/0 min, which reflects the finding that at this time point both PsVs and HS preferentially locate at
382 the cell periphery (Figure 6C, for PCC values of flipped images see Supplementary Figure 8). Over time,
383 the accumulated PsVs diminish due to translocation, which is accompanied by a PCC approaching zero,
384 the same value as in the control (Figure 6C). Additionally, we analyze the PCC between PsVs and HS
385 specifically in the cell body region, excluding the cell periphery (Figure 6D). For the control, the PCC in
386 the cell body region ranges between 0 and 0.05. After CytD, we observe an increase in the PCC from
387 0 min to 30 min and a decrease from 30 min to 180 min (for PCC values of flipped images see
388 Supplementary Figure 8).

389 When analyzing the PsVs closely associating with HS, at 0 min, CytD increases the fraction of
390 PsVs associated with HS more than 3-fold. Over the next 180 min, this fraction gradually decreases
391 until it is equal to the control value (Figure 6E).

392 Altogether, the analysis of the PCC between HS and PsVs (Figure 6C) along with the fraction
393 of closely HS associated PsVs (Figure 6E) indicates that CytD treatment increases HS/PsV association
394 at 0 min, likely because PsVs remain accumulated in the ECM. After CytD removal, this association
395 diminishes. A transient increase in PCC is observed at 30 min specifically in the region of the cell body
396 (Figure 6D) which likely reflects the translocation of HS-coated virions to the cell body. However, this
397 association also diminishes over the subsequent 150 min, suggesting that an increasing number of
398 PsVs are no longer associated with HS – likely due to progressive loss of the HS coat over time.
399 Alternatively, PsVs just may disappear after internalization.

400 Next, for each PsV we plot the 'distance to the next nearest Itgα6 maximum' against 'the
401 distance to the next nearest HS maximum' (Figure 7). In the control, the distances remain unchanged
402 over the entire observation time; 59% - 65% of the PsVs are at a short distance (< 250 nm) to both
403 Itgα6 and HS (Figure 7B, black; see also Supplementary Table 1), 12 - 15% are at a short distance (<
404 250 nm) to HS but not to Itgα6 (> 250 nm) (Figure 7B, green; see also dashed green box in Figure 9
405 marking PsVs in the ECM). Also, the distance plots are in line with the idea that the distance patterns
406 of PsVs in untreated cells do not change over the 180 min observation time (Figure 7C, please compare
407 the upper distance plots from left to right). In cells treated with CytD, a larger fraction of PsVs is
408 accumulated at the periphery at the 0 min time point, which is reflected in a larger fraction (46% as
409 opposed to 12% in the control; Figure 7B, green; Supplementary Table 1) of PsVs with a short distance
410 (< 250 nm) to HS but not to Itgα6. Over time, the PsVs in the CytD treated cells acquire a shorter
411 distance to Itgα6 and a larger distance to HS (Figure 7C, lower row). The population with short

412 distances to HS and large ones to Itgα6 strongly diminishes from 46% to 11% (Figure 7B, CytD, green).
413 After 180 min, the distances are similar to the untreated control. Between CytD/60 min and
414 CytD/180 min, the fraction of PsVs with a large distance (> 250 nm) to HS and a short distance (<
415 250 nm) to Itgα6, representing PsVs at the cell body without HS (see also dashed magenta box in
416 Figure 9), increases from 9.6% to 25.2% (Figure 7B, magenta). This is inconsistent with the idea of
417 endocytosis of HS-coated PsVs that would only diminish short distances to Itgα6 but not create long
418 distances to HS, which is what we observe. The observation supports the idea that PsVs lose their HS
419 coat after translocating to the cell surface, which is also supported by the transient increase in the PCC
420 between HS and PsVs of the cell body at 30 min (Figure 6D).

421 The movement of HS towards the cell body after removal of CytD, which indirectly
422 demonstrates that PsVs are coated with HS, is suggested by a shortening of the HS-Itgα6 distance over
423 time (Supplementary Figure 8D). Moreover, the PCC between PsVs and HS in the cell body area
424 increases (Figure 6D). Altogether, the data suggest that HS-coated PsVs migrate towards the cell body.
425 A large fraction of translocating PsVs sheds HS within one hour after removing CytD (Figure 7C, lower
426 panels, showing increasing PsV-HS distances). This is the time window where we notice the occurrence
427 of endocytic PsV/CD151 structures (see above and Supplementary Figure 5).

428 Actin retrograde transport, which underlies the here observed virion transport, is the
429 integrative result of three components (***Schelhaas et al., 2008; Smith et al., 2008***). On the one side,
430 actin filaments in the cell periphery are pushed into the cell body area when actin polymerizes at their
431 tips. The retrograde filament movement causes tension and is facilitated by F-actin degradation
432 opposed to the side of F-actin growth. Moreover, the motor protein myosin II exerts force on actin
433 filaments, pulling those towards the cell body. As CytD broadly interferes with F-actin dependent
434 processes, we investigated the effects upon inhibition of only one of the three components, namely
435 the myosin II mediated retrograde movement towards the cell body. Instead of CytD, we employed in
436 the 5 h preincubation the myosin II inhibitor blebbistatin. For the control (0 min), we show in Figure
437 8A one example of a cell with comparatively many PsVs at the periphery (as mentioned above, the
438 PsV pattern is highly variable) to better illustrate the difference to the PsV pattern occasionally seen
439 with blebbistatin. After blebbistatin treatment (0 min), PsVs are still distal to the cell body but less
440 dispersed than after CytD treatment, seemingly as if translocation started but stopped in the midst of
441 the pathway (Figure 8A, blebbistatin). The PCC between PsVs and HS, like after CytD (Figure 6C), is
442 elevated after blebbistatin, albeit the effect is not significant (Figure 8C). The cell body PCC, is not at
443 30 min (CytD) but already at 0 min elevated (compare Figure 6D to Figure 8D), which can be explained
444 by partial translocation. This is further supported by the fact that only 8% of PsVs are closely associated
445 with HS (Figure 8E; blebbistatin, 0 min) compared to 15% after CytD treatment (Figure 6E; 0 min).

446 Furthermore, after 0 min PsV incubation with blebbistatin we observe no effect on the HS intensity
447 (compare Figure 8B to Figure 3B and Figure 6B). Hence, in contrast to CytD, blebbistatin does not trap
448 the PsVs in the ECM where they associate with HS, but ongoing actin polymerization pushes actin
449 filaments along with PsVs towards the cell body.
450
451
452 **Discussion**
453 In this study, we investigate the early events of HPV16 infection preceding virus endocytosis.
454 Our findings reveal that actin dynamics of filopodia, rather than passive virion diffusion, are crucial for
455 releasing HS-coated virus particles from the adhesive ECM and translocating them to the cell body.
456 When actin-dependent processes are inhibited by CytD, HS-coated virus particles remain trapped in
457 the ECM, allowing for a more synchronized observation of the infection process. Once the transfer is
458 no longer blocked, PsVs rapidly migrate toward the cell body, associate with CD151, and shed their
459 HS-coat before endocytosis.
460
461 *A reversible blocking of PsV translocation from the ECM to the cell body by CytD*
462 Many viruses use cell surface HS for primary attachment, including herpes simplex virus
463 type 1, human cytomegalovirus, human immunodeficiency virus type 1, adenovirus type 2, dengue
464 virus, hepatitis B virus, and vaccinia virus (***Cagno et al., 2019; Giroglou et al., 2001; Tian et al., 2021***).
465 HPVs could be different as they bind as well to HS of the extracellular basement membrane, at least
466 *in vivo* during the wounding and healing processes required for infection (***Day and Schelhaas, 2014;***
467 ***Kines et al., 2009; Ozbun and Campos, 2021; Schiller et al., 2010***).
468 By treating cells with CytD, we block actin-mediated transport, leading to a 6-fold
469 accumulation of PsVs at the cell periphery after 5 hours (Figure 4B). After CytD removal, infectivity is
470 only moderately reduced (29%) (Figure 1E), suggesting that the treatment is reversible and only
471 slightly harmful, if at all.
472 Upon CytD washout, PsVs translocate to the cell body with a half-time of ≈15 minutes, as
473 suggested by the diminishment of accumulated PsVs at the periphery. As mentioned above, the half-
474 time could be longer if cell spreading is in part responsible for the translocation of PsVs onto the cell
475 body. However, we assume that this is rather unlikely, as cell spreading would increase the PCC
476 between PsVs and F-actin under a condition where filopodia mediated transport is blocked but not
477 cell spreading, which is not the case (Figure 2B and D, CytD/leupeptin). Within this 15 min time frame,
478 PsVs associate more strongly with CD151. It is in principle possible that along with CytD removal ECM-

479 accumulated PsVs are merely washed off. However, after only 15 min, the effect of this could not have
480 been very strong, considering the still 6-fold accumulation of PsVs after the 5 h incubation with CytD.
481 Furthermore, CytD pre-treatment appears to synchronize uptake: We observe endocytic
482 structures after CytD treatment more frequently (for examples see Supplementary Figure 5) and the
483 CD151 intensity diminishes over time only after the CytD treatment (Figure 5B). We therefore
484 conclude that the processing of the PsVs in the ECM is contributing to desynchronization and is largely
485 completed after the 5 h pre-incubation with CytD. We estimate that about 6-fold more PsVs (Figure
486 2B) translocate to the cell surface in a coordinated fashion after CytD removal, which likely enhances
487 the number of endocytic events compared to untreated controls.
488
489 *The role of actin-driven virion transport*
490 The strong electrostatic interaction between HPV and HS implies that some processing — via
491 HS cleavage or structural capsid changes — is a prerequisite for the release of virions from the ECM.
492 CytD likely does not inhibit HS processing (***Jamieson et al., 2021***; see also Supplementary Figure 2) nor
493 is it likely to inhibit KLK8. Therefore, we assume that PsVs are primed after 5 h of incubation with CytD.
494 They may remain associated via weaker interactions, and actin-driven transport is required for pulling
495 the HS-coated virions out of the sticky matrix towards the cell body. Sticky PsV aggregations that are
496 released from HeLa cell surface after binding and blocking of the subsequent entry pathway have been
497 observed earlier and might reflect similar HS/PsV-stuctures (***Mikuličić et al., 2025***). Alternatively, an
498 ECM bound virion is not exposed to all processing factors at the same time. In this case, migration
499 through the ECM is additionally required to establish, one by one, contact with all processing enzymes
500 involved. Once the fully processed virions have reached the cell surface, detachment from the ECM
501 may be facilitated by new bonds established between the PsVs and cell surface receptors. Now, the
502 PsVs and cell surface receptors move towards the central cell body by intracellular dynamics which
503 results in CD151 accumulation at virus binding sites and ultimately endocytosis (see Figure 5 as well
504 as Supplementary Figure 5).
505 Both CytD and blebbistatin increase PsV-HS colocalization, but blebbistatin allows partial
506 translocation (compare Figure 6C and Figure 8C as well as Figure 6D and Figure 8D), indicating that
507 actin retrograde flow initiates movement, while myosin II contributes to sustained transport. As a
508 result, virus movement can proceed to some extent after blebbistatin treatment. However, the
509 subsequent blocking of transport at later time points reflects the inhibition of myosin II, which
510 eventually disrupts the cytoskeletal dynamics and force generation that is necessary for sustained
511 transport. In contrast, CytD directly interferes with actin polymerization, leading to an earlier and

512 more persistent blocking of virus transport due to structural disruption of the filopodial tracks
513 themselves.
514 Altogether, our findings support earlier reports showing that HPV utilizes filopodia for cell
515 entry, migrating at several micrometers per minute (***Schelhaas et al., 2008; Smith et al., 2008***). This
516 translocation is fast compared to the entire infection process and therefore cannot largely contribute
517 to the asynchronous HPV uptake. Since we use polarized cells, PsVs hardly bind to the cell surface
518 directly (Supplementary Figure 1). Therefore, the actin-driven virion transport plays a decisive role in
519 HPV infection of isolated HaCaT cells, which cannot be modelled in nonpolarized cells, where PsVs can
520 bind to the entire cell surface.
521
522 *HaCaT cells as model system in HPV infection*
523 Inhibition of HPV16 PsV transport diminishes infection only of subconfluent but not of
524 confluent HaCaT cells by about 50% (***Schelhaas et al., 2008***). Therefore, actin-dependent translocation
525 along protrusions may be dispensable for infection at a high cell density (***Schelhaas et al., 2008***) and
526 merely increases the exposure of cells to virions (***Smith et al., 2008***). However, this increased exposure
527 could be relevant *in vivo*, as wounding of the epidermis results in upregulation of filopodia formation
528 (***Vasioukhin et al., 2000***). Filopodia usage not only facilitates infection but also increases the likelihood
529 of virions to reach their target cells during wound healing, namely the filopodia-rich basal dividing
530 cells. In fact, several types of viruses exploit filopodia during virus entry (***Chang et al., 2016***), hinting
531 at the possibility that for HPV and other types of viruses actin-driven virion transport may play a more
532 important role than it is currently assumed. If this is the case, sub-confluent HaCaT cells, or even better
533 single HaCaT cells, would be an ideal model system for the study of these very early infection steps
534 that involve ECM attachment and subsequent filopodia-dependent transport. As shown in
535 Supplementary Figure 1, HaCaT cells have many binding sites for the HPV16 PsVs. However, as they
536 are polarized and the binding receptors are only at the basal membrane, they remain relatively
537 inaccessible by diffusion. Therefore, the ECM binding that is also observed *in vivo* (***Day and Schelhaas,***
538 ***2014***) and subsequent transport via filopodia are used upon infection of HaCaT cells that locate at the
539 periphery of cell patches. Here, PsVs bind to the ECM which strongly enhances infection of primary
540 keratinocytes (***Bienkowska-Haba et al., 2018***). In contrast, HPV can readily bind to HSPGs on the cell
541 surface of nonpolarized cells, and by this bypasses ECM mediated virus priming and the filopodia
542 dependency. We propose that HaCaT cells are a valuable system for studying the very early events in
543 HPV infection that allows for dissecting capsid interaction with ECM resident priming factors and cell
544 surface receptors.
545

546 *Translocating PsVs are decorated with HS which they lose over time*

547 CytD treatment increases the HS signal when PsVs are present (Figure 3B and 6B). A
548 relationship between PsVs and HS cleavage products has been previously suggested (***Ozbun and***
549 ***Campos, 2021; Surviladze et al., 2012***), and we propose that our data is in line with these previous
550 observations. It should be noted that under conditions without the 5 h CytD blocking, PsVs may only
551 briefly reside in the ECM and as a result are less decorated with HS. Hence, under our assay conditions
552 the HS decoration of virions may be enhanced in comparison to other assays.

553 At the 0 min time point post-CytD, 15% of the PsVs are closely associated with HS (Figure 6E),
554 but this fraction declines to 4.3% by 180 min. Considering the important role of HS as a primary
555 attachment site, the fraction of 15% appears unexpectedly small. There are multiple possible
556 explanations for underestimating the number of PsVs closely associated with HS. One contributing
557 factor may be that accumulated PsVs are not well-resolved (see above), which results in an
558 underestimation of HS associated PsVs in particular at CytD/0 min. Other explanations include that
559 the HS antibody does not reach all HS epitopes in the dense matrix. Yet another explanation could be
560 that PsV binding to HS and antibody binding to HS is sometimes mutually exclusive, a hypothesis which
561 is supported by data showing that the HPV capsid possesses multiple HS binding sites (***Dasgupta et***
562 ***al., 2011; Richards et al., 2013***). Together, our data suggests that PsVs initially translocate with HS
563 attached and then shed it, potentially either upon receptor binding or further capsid rearrangement.
564 These observations are in line with a previous study showing reduced HS colocalization during
565 productive infection (***Selinka et al., 2007***).

566 The initial HS-coat may facilitate the formation of a complex with PsVs and cell surface
567 receptors such as integrins or growth factor receptors (GFRs) (***Ballut et al., 2013; Pellegrini, 2001***).
568 This could facilitate receptor clustering and engagement as shown previously for coronavirus infection
569 (***Bugatti et al., 2025; Clausen et al., 2020; Zhang et al., 2023***), as well as the binding of signaling
570 molecules to the cell surface (***Miladinova et al., 2022***). Here, CD151 may support receptor clustering
571 by binding to both integrins and GFRs (***Hemler, 2005; Mikuličić et al., 2019***). In addition, earlier studies
572 suggested that cofactors like laminin-332 and growth factors further stabilize these interactions (***Culp***
573 ***et al., 2006; Mikuličić et al., 2019; Richards et al., 2014; Surviladze et al., 2012***). Furthermore, the
574 HPV capsid has multiple binding sites for distinct functions (***Richards et al., 2013***) which supports the
575 idea that HS fulfills several roles during viral entry — first by promoting capsid attachment, then
576 inducing conformational changes, and finally by assisting in receptor engagement and clustering.
577 However, HS cleavage alone is not sufficient for ECM release; active transport and capsid priming
578 remain essential (see leupeptin effect in Figure 2B and D). Diffusion may account for some virion
579 movement, but filopodia-mediated transport dominates in this context.

580

581 *PsV-CD151 association is an early contact at the cell surface*

582 CD151 is a known mediator of HPV entry (***Scheffer et al., 2013; Spoden et al., 2008***). Our data
583 shows that about 10% of the PsVs are closely associated with CD151 at all post-translocation time
584 points. This fraction is lower at 0 min post-CytD (Figure 5D, see also lower PCC in Figure 5C), indicating
585 that actin disruption impairs initial CD151 engagement. Hence, the data suggest that PsVs establish
586 contact to CD151 assemblies shortly after translocation to the cell surface, and from then on, the
587 fraction of closely associated PsVs remains constant. At first glance this implies that, after the initial
588 formation of the PsV-CD151 assemblies, they do not change in nature. However, we observe
589 agglomerated CD151 maxima (locally patched maxima) close to PsVs at later time points that likely
590 are endocytic structures (see arrow in Figure 5A, Supplementary Figure 5). This agglomeration process
591 is not detected in our analysis as we only determine the next nearest CD151 assembly. Some further
592 CD151 reorganization into larger entry platforms has been previously observed (***Florin and Lang,***
593 ***2018***). This is in accordance with the observation that virions enter the cell in crowds with many of
594 them occupying one endocytic organelle (***Schelhaas et al., 2012***).

595 For the PsVs closely associated with CD151, one may have expected a larger fraction than
596 10%. Given that PsVs are not supposed to bind directly to CD151 and that CD151 is likely part of a
597 larger membrane structure, like a tetraspanin enriched microdomain, our ≤ 80 nm distance criteria
598 may be too short and by this we underestimate the association frequency. Altogether, we propose
599 that an early contact between PsVs and the cell surface involves an assembly defined by CD151 (Figure
600 9).

601

602 *Integration of our data into the HPV infection cascade*

603 HPV infection is the result of several steps, starting with the initial binding of virions via
604 electrostatic and polar interactions (***Dasgupta et al., 2011***) to the primary attachment site HS
605 (***Richards et al., 2013***), which induces capsid modification (***Cerqueira et al., 2015; Feng et al., 2024***)
606 and HS cleavage (***Surviladze et al., 2015***), enabling the virion to be released from the ECM or the
607 glycocalyx. Next, virions bind to the cell surface to a secondary receptor complex that forms over time,
608 and become internalized via endocytosis, before they are trafficked to the nucleus (***Mikuličić et al.,***
609 ***2021; Ozbun and Campos, 2021***). Regarding the transition from the primary attachment site to cell
610 surface binding, as already outlined in the introduction, two models are discussed. In one model,
611 proteases cleave the capsid proteins. After priming, the capsids are structurally modified and the
612 virion can dissociate from its HS attachment site. It has been suggested that capsid priming is mediated
613 by KLK8 (***Cerqueira et al., 2015***) and furin (***Richards et al., 2006***). In our system, KLK8 inhibition blocks

614 PsV transport, while furin inhibition has some effect that, however, cannot be detected in this analysis
615 (Figure 2) suggesting furin engagement at later steps in the infection cascade. This is in line with earlier
616 *in vitro* studies on the role of cell surface furin (***Day et al., 2008; Day and Schiller, 2009; Surviladze et***
617 ***al., 2015***). In any case, our results align with both models of ECM detachment: one involving HS
618 cleavage (HS co-transfer) and another involving capsid modification (by e.g., KLK8).
619 We propose that after 5 h of CytD treatment, glycan-induced structural activation as well as
620 capsid processing by proteases such as KLK8 of the capsid and HS cleavage essentially are completed
621 ((i) in Figure 9). Subsequently, (ii) the HS decorated virion is transported from the ECM to the cell body
622 on filopodia, which takes about 15 min. In a time window of 30 min, PsV-CD151 association occurs.
623 (iii) In the samples recorded 30 – 180 min after CytD wash off, we observe that PsVs lose their HS-coat,
624 and individual PsV-CD151 assemblies seem to merge into larger structures that are subsequently
625 endocytosed. This model highlights the role of ECM interactions, actin dynamics, and receptor
626 engagement in HPV16 entry.
627
628
629 **Materials and Methods**
630 *Antibodies and PsVs*
631 We used the following primary antibodies in immunostainings of proteins. For the capsid
632 protein L1, a rabbit polyclonal antibody (pAb) K75 (diluted 1:1000) as described previously (***Knappe et***
633 ***al., 2007; Rommel et al., 2005***), for CD151 a mouse monoclonal antibody (mAb) (1:200) (Biorad, cat#
634 MCA1856GA), and for Itgα6 a rabbit polyclonal antibody (1:200) (Invitrogen, cat# PA5-12334) were
635 used. For Heparan sulfate (HS) a mouse IgM monoclonal antibody (1:200) (amsbio, cat# 370255-S) was
636 used that reacts with an epitope in native heparan sulfate chains and not with hyaluronate,
637 chondroitin or DNA, and poorly with heparin (mAb 10E4 (***David et al., 1992***)). For HS neo-epitope
638 (***Yokoyama et al., 1999***) detection, a mouse monoclonal antibody (1:200) (amsbio, cat#370260-S) was
639 used that reacts only with heparitinase-treated heparan sulfate chains, proteoglycans, or tissue
640 sections, and not with heparinase treated HSPGs. The antibody recognizes desaturated uronic acid
641 residues (mAb 3G10 (***David et al., 1992***)). As secondary antibodies we used a STAR GREEN-coupled
642 goat-anti-rabbit (1:200) (Abberior, cat# STGREEN-1002-500UG), an AlexaFluor 594-coupled donkey-
643 anti-rabbit (1:200) (Invitrogen, cat# A21207), an AlexaFluor 594-coupled donkey-anti-mouse (1:200)
644 (Invitrogen, cat# A21203), an AlexaFluor 594-coupled donkey-anti-mouse IgM (1:200) (Invitrogen,
645 cat# A21044), a STAR RED-coupled goat-anti-mouse (1:200) (Abberior, cat# STRED-1001-500UG) and
646 a STAR RED-coupled goat-anti-rabbit (1:200) (Abberior, cat# STRED-1002-500UG). Additionally,
647 phalloidin iFluor488 (1:1000 of ready to use solution) (abcam, cat# ab176753) or phalloidin iFluor647

648 (1:1000) (abcam, cat# ab176759) was used to stain F-actin. Staining of the PsV plasmid DNA was
649 performed by click-labeling according to the manufacturer's instructions with the dye 6-FAM Azide
650 (Baseclick EdU 488 kit, Carl Roth, cat# 1Y67.1).

651 HPV16 PsVs were produced following established procedures (***Buck et al., 2004; Spoden et***
652 ***al., 2012***). HEK293TT cells were cultured in 175 cm^2 flasks and transfected with polyethylenimine (PEI),
653 using equimolar amounts of codon-optimized HPV16 L1/L2 (pShell-16L1wt-16L2wt) and a reporter
654 plasmid (pGL4.20-puro-HPV16 LCR (***Wüstenhagen et al., 2018***)). For the production of 5-ethynyl-2'-
655 deoxyuridine (EdU)-labeled PsVs, the culture medium was replaced 5 hours post-transfection with
656 fresh medium containing 30 µM EdU. After 48 hours, cells were harvested, centrifuged, and washed
657 twice with phosphate-buffered saline (PBS) supplemented with 9.5 mM $MgCl_2$ (1x PBS/ $MgCl_2$). After
658 the final centrifugation, the pellet was resuspended in 1x PBS/ $MgCl_2$ containing 0.5% Brij58 (Sigma-
659 Aldrich), and 250 units Benzonase (Merck Millipore), and incubated at 37°C for 24 hours on a rotating
660 platform. Subsequently, lysates were chilled on ice and the NaCl concentration was adjusted to 0.85
661 M. After clarification by centrifugation, the supernatant was loaded onto an iodixanol (Optiprep)
662 gradient consisting of 39%, 33%, and 27% layers (bottom to top). Gradients were equilibrated for 90
663 minutes at room temperature before ultracentrifugation at 55,000 rpm for 3.5 hours at 16°C. Fifteen
664 fractions of 300 µl each were collected from the top and analyzed via luciferase reporter assay to
665 identify peak fractions. PsV titers were determined based on packaged genomes (viral genome
666 equivalents, vge) as previously described (***Spoden et al., 2012***). The concentrations of stock solutions
667 were 7.7 x 10^6 vge/µl (for microscopy experiments) and 14.1 x 10^6 vge/µl (for the luciferase assay).
668
669 *Cell culture*

670 For microscopy, human immortalized keratinocytes (HaCaTs) (Cell Lines Services, Eppelheim,
671 Germany) were cultured in high glucose Dulbecco's modified Eagle's medium (DMEM + GlutaMAX,
672 Gibco, cat# 61965-026) supplemented with 10% FBS (PAN Biotech, cat# P30-3031) and 1%
673 Penicillin/Streptomycin (10,000 U/ml Penicillin, 10 mg/ml Streptomycin; PAN Biotech, cat# P06-
674 07100) at 37 °C with 5% CO_2. For the luciferase infection assay, cells were grown at 37°C and 5% CO_2
675 in Dulbecco's modified Eagle's medium (DMEM + GlutaMAX, Thermo Fisher Scientific), supplemented
676 with 10% FBS (Sigma-Aldrich), 1% minimum essential medium non-essential amino acids (MEM non-
677 essential amino acids (Thermo Fisher Scientific)), and 5 µg/ml ciprofloxacin (Fresenius Kabi). For
678 experiments, the antibiotics in the medium were omitted.
679
680 *Sample preparation and immunostaining*

681 About 150,000 HaCaT cells were plated onto 25 mm diameter poly-L-lysine (PLL) coated
682 (100 µg/ml PLL for 30 min) glass coverslips in 6-well plates and incubated for 24 h at 37°C and 5% CO_2.
683 The next day, cells were incubated at 37°C and 5% CO_2 for 5 h with PsVs (50 vge/plated cell) and
684 10 µg/ml cytochalasin D (CytD; stock solution 10 mg/ml in dimethyl sulfoxide (DMSO)) (Life
685 Technologies, cat# PHZ1063) or 30 µM (−)-blebbistatin (stock solution 13.68 mM in DMSO) (Sigma-
686 Aldrich, cat# B0560-1MG) in DMEM supplemented with 10% FBS. For controls, we added the same
687 amount of DMSO without CytD or blebbistatin. Cells were washed with PBS (137 mM NaCl, 2.7 mM
688 KCl, 1.76 mM KH_2PO_4, 10 mM Na_2HPO_4, pH 7.4) and fresh DMEM supplemented with 10% FBS was
689 added. Cells were incubated further at 37°C and 5% CO_2 for 0 min (here the medium was added
690 followed by immediate removal), 15 min, 30 min, 60 min and 180 min.
691 In another set of experiments, about 150,000 HaCaT cells were plated onto 25 mm diameter
692 PLL coated glass coverslips in 6-well plates and incubated for 24 h at 37°C and 5% CO_2. The next day,
693 cells were incubated at 37°C and 5% CO_2 for 5 h with PsVs (50 vge/plated cell) and 10 µg/ml CytD
694 either together with 100 µM leupeptin (stock solution 100 mM in ddH_2O) (Carl Roth, cat# CN33.1) or
695 5 µM Furin inhibitor I (stock solution 5 mM in DMSO) (Sigma-Aldrich, cat# 344930-1MG) in DMEM
696 supplemented with 10% FBS. For controls, we used only 10 µg/ml CytD. Cells were washed with PBS
697 and fresh DMEM supplemented with 10% FBS was added. Cells were incubated further at 37°C and
698 5% CO_2 for 0 min, 30 min and 60 min.
699 To analyze PsV binding to detached HaCaT cells, about 350,000 HaCaT cells per well were
700 plated in 6-well plates and incubated for 24 h at 37°C and 5% CO_2. The next day, cells were detached
701 by a 15 min incubation with 10 mM EDTA (in PBS, pH 7.4) at 37°C and 5% CO_2. Detached cells were
702 collected and incubated with 50 vg/cell in DMEM supplemented with 10% FBS under constant rotation
703 at 4 °C for 1 h. Cells were washed three times with PBS at 4 °C to remove any unbound PsVs. Then,
704 cells were seeded onto 25 mm diameter PLL coated glass coverslips in 6-well plates and incubated for
705 1 h at 37°C and 5% CO_2.
706 Before staining, cells were washed twice with PBS and fixed at room temperature (RT) with
707 4% PFA in PBS for 30 min, unless membrane sheets were generated. In this case, the coverslips were
708 placed in ice cold sonication buffer (120 mM KGlu, 20 mM KAc, 10 mM EGTA, 20 mM HEPES, pH 7.2)
709 and a 100 ms ultrasound pulse at 100% power was applied. This was repeated until in total about 10
710 pulses were applied at different locations of the coverslip. Then, membrane sheets were fixed like
711 cells at RT with 4% PFA in PBS for 30 min. PFA was removed, and residual PFA was quenched by 50 mM
712 NH_4Cl in PBS for 30 min. Afterwards, samples were blocked with 3% BSA in PBS for 30 min. Staining of
713 PsVs was performed by click-labeling with the dye 6-FAM for 30 min at RT according to the
714 manufacturer's instructions. Then, samples were washed three times with PBS. In case of no PsV

715 labeling by click-chemistry, directly after blocking, the respective primary antibodies were added:
716 mouse IgM mAb against HS (1:200), mouse mAb against Δ-HS (1:200), rabbit pAb against Itgα6 (1:200),
717 mouse mAb against CD151 (1:200) and rabbit pAb K75 against L1 (1:1000) in 3% BSA in PBS for 2 h.
718 Samples were washed three times with PBS before adding the respective secondary antibodies and
719 fluorescent labelled phalloidins in 3% BSA in PBS for 1 h: for HS we added AlexaFluor 594 coupled to
720 donkey-anti-mouse IgM (1:200), for Δ-HS AlexaFluor 594 coupled to donkey-anti-mouse (1:200), for
721 Itgα6 STAR RED coupled to goat-anti-rabbit (1:200), for CD151 AlexaFluor 594 coupled to donkey-anti-
722 mouse (1:200) or STAR RED coupled to goat-anti-mouse (1:200), for L1 AlexaFluor 594 coupled to
723 donkey-anti-rabbit (1:200) or STAR GREEN coupled to goat-anti-rabbit (1:200) and for F-actin
724 phalloidin iFluor488 (1:1000) or phalloidin iFluor647 (1:1000). Afterwards, samples were washed three
725 times with PBS, followed by mounting of the coverslips onto microscopy slides using ProLong Gold
726 antifade mounting medium (Invitrogen, cat# P36930).
727
728 *Confocal and STED microscopy*
729 For confocal and STED microscopy, samples were imaged employing a 4-channel STED
730 microscope from Abberior Instruments. The microscope is based on an Olympus IX83 confocal
731 microscope equipped with an UPlanSApo 100x (1.4 NA) objective (Olympus, Tokyo, Japan). Confocal
732 and STED micrographs were recorded simultaneously. For confocal imaging, a 488 nm laser was used
733 for the excitation of 6-FAM, STAR GREEN and phalloidin iFluor488, and emission was detected at 500–
734 550 nm. For STED imaging, a 561 nm laser (at 45%) was used for the excitation of AlexaFluor 594
735 (detection at 580–630 nm) and a 640 nm laser (at 45%) for the excitation of STAR RED and iFluor647-
736 labelled phalloidin (detection at 650-720 nm), in combination with a 775 nm laser for depletion (at
737 45%). The pixel size was set to 25 nm, for overview images a pixel size of 250 nm was used.
738
739 *Analysis of confocal and STED micrographs*
740 Images were analyzed using Fiji ImageJ (***Schindelin et al., 2012***) in combination with a custom
741 written macro, essentially as described previously (***Schmidt et al., 2024***). When analyzing double
742 stainings of Alexa594 (red channel) and STAR RED (long red channel), we corrected for crosstalk from
743 the red into the long red channel by subtracting 40% of the intensity of the red channel image from
744 the long red channel image.
745 First, images were smoothed with a Gaussian blur to improve maxima detection. For confocal
746 PsV-DNA micrographs, we employed a Gaussian blur of $\sigma = 1$, and for confocal PsV-L1 and STED
747 micrographs a Gaussian blur of $\sigma = 0.5$. Local maxima were detected using the 'Find Maxima' function
748 (noise tolerance 60 for L1 if stained together with phalloidin iFluor488, and 80 if stained together with

749 CD151, HS, or phalloidin iFluor647, 3 for click-labeled PsVs, 8 for CD151, 6 for HS and 15 for Itgα6),
750 yielding maxima positions in pixel positions. For analysis, regions of interest (ROIs) were defined (for
751 details see figure legends).

752 In order to define the cell border region (Supplementary Figure 3B), the ImageJ 'Make Binary'
753 function was used on CD151 STED micrographs for generating a binary mask. When possible, the
754 'Wand' tool was used to further outline the area covered by the cell, otherwise the same was done
755 manually using the original micrograph as a reference. From the outline in the binary mask, a ROI was
756 created, that was then filled in white with the 'Flood Fill' Tool. The ROI was shrunk to a 20-pixel broad
757 strip, and cleared outside of the strip, what leaves a 20-pixel broad, closed ribbon marking the
758 intracellular side of the cell border that, however, exhibits arbitrary edges produced in the process
759 above. These edges were removed by manual adjustments with the 'Pencil' tool and the clear
760 function. Afterwards, the ROI defines the intracellular side of the cell border. The ROI was
761 symmetrically broadened by 40 pixels (using the 'Enlarge' function). From the now at least 60 pixels
762 broad ROI, approximately two thirds covered the intracellular and one third the extracellular side. In
763 this ROI, using the ImageJ 'Find Maxima' function, PsV-L1 maxima were detected (at a noise tolerance
764 of 80) with a custom written macro in ImageJ both in the cell border region ROI and in a ROI covering
765 the entire micrograph (excluding a 2-pixel edge). From these values, the percentage of PsVs within the
766 cell border region was calculated.

767 For measuring intensity over time, we measured in the ROI the mean gray value. For
768 background correction, we subtracted the mean gray value measured in a ROI next to the cell.

769 For measuring maxima intensity, a ROI with a diameter of 125 nm (5 pixels) was placed onto
770 the determined maxima positions (see above). Using these ROIs, the average mean gray value of each
771 maximum was measured. The average background mean gray value was measured in a ROI placed
772 next to the cell and subtracted from the average mean gray value of the maxima. For each membrane
773 sheet, the average maxima intensity was calculated, followed by averaging of the values of the
774 membrane sheets.

775 To measure the shortest distance, e.g., between PsV and CD151 maxima, as a quality control
776 for the PsV maxima (CD151 maxima do not undergo the quality control step) we placed onto each
777 maximum position a horizontal and a vertical linescan (31 pixels long × 3 pixels width). Afterwards, we
778 fitted a Gaussian distribution to the intensity distribution of each maximum. Only if at least one of the
779 fits exhibits a fit quality of $R^2 > 0.8$ and if the Gaussian maximum located central to the intensity
780 distribution the maximum was included in the further analysis. Moreover, using a 125 nm ROI at the
781 PsV and CD151 maxima positions, the center of mass of fluorescence was determined, yielding the

782 maxima positions in sub-pixels. Based on these positions we further calculated the shortest distance
783 of a PsV maximum to the nearest CD151 maximum.
784 Using the shortest distances, we either calculated the fraction of closely associated PsVs (PsVs
785 with a distance ≤ 80 nm to e.g., CD151) over time, or the average shortest distance over time. The
786 fraction of closely associated PsVs was corrected for random background association that increases
787 with the maxima density. The relationship between background association and maxima density was
788 expressed by a linear equation obtained from the same images re-analyzed after flipping them
789 horizontally and vertically (see e.g., Supplementary Figure 7).
790 The Pearson correlation coefficient (PCC) was calculated with a custom written macro in
791 ImageJ. As a control, we performed the analysis on horizontally and vertically flipped ROI-defined
792 images as well (see e.g., Supplementary Figure 6A). The cell body PCC between PsVs and HS is
793 measured in smaller ROIs covering exclusively the cell body region (this is confirmed with the Itgα6 or
794 F-actin image as reference).
795 Per condition and biological replicate, 14 - 15 images were analyzed and values were
796 averaged. For images from one set of experiments, in the figure the same channels are shown at the
797 same settings of brightness and contrast, if not stated otherwise.
798
799 *Epi-fluorescence microscopy and image analysis*
800 For epifluorescence microscopy, we used microscopic equipment and settings as previously
801 described (***Homsi et al., 2014***) except of the illumination system, which was replaced by a SPECTRA X
802 Light engine; Lumencor, Beaverton, OR, USA). In brief, PFA-fixed cells were imaged in a chamber filled
803 with 1 ml of PBS to which 50 µl of a saturated solution of TMA-DPH [1-(4-tri-methyl-ammonium-
804 phenyl)-6-phenyl-1,3,5-hexatriene-p-toluenesulfonate (T204; Thermofisher)] in PBS was added, for
805 visualizing the membranes in the blue channel. PsVs, HS and Itgα6 were imaged in the green, red and
806 far-red channels, respectively.
807 For analysis, rectangular ROIs of ≈ 45 x 10^3 pixel were placed onto the cell body such that
808 approximately one half of the ROI covers the ECM area and the other one the cell body. The cell
809 periphery was defined using the TMA-DPH image from which a binary mask was created. With
810 reference to the binary mask, a band of up to 30 pixels width was created beginning at the cell body
811 and reaching out towards the cell periphery. Using this ROI, in the PsV-DNA image the size of the ROI
812 and the mean gray values were measured from which the integrated intensities were calculated after
813 background correction.
814
815 *Luciferase infection assay*

816 HaCaT cells were grown in 24-well plates and allowed to adhere overnight. The following day,
817 cells were treated with HPV16 PsVs at a concentration of approximately 100 vge per cell, in the
818 presence or absence of 10 µg/ml cytochalasin D (CytD) in DMSO or an equivalent amount of DMSO
819 (Control). In one condition, PsVs/CytD were applied for 5 hours, after which the medium was replaced
820 with fresh medium lacking the compounds, and incubation was continued for additional 19 hours (in
821 total 24 h). In another condition, cells were exposed to PsVs/CytD continuously for the full 24 h period.
822 Then, cells were washed with PBS and lysed using 1 x Cell Culture Lysis Reagent (Promega, cat# E153A).
823 Following high-speed centrifugation, luciferase activity in the cleared lysates was quantified using an
824 LB 942 Tristar 3 Multimode Microplate Reader (Berthold Technologies). Cytotoxic effects,
825 accompanied by a loss of membrane integrity (indicated by released lactate dehydrogenase (LDH)),
826 were determined by measuring the LDH levels in the cell lysates. LDH activity was assessed using the
827 CytoTox-ONE Homogeneous Membrane Integrity Assay (Promega, cat# G7891). LDH fluorescence was
828 quantified according to the manufacturer's instructions using the LB 942 Tristar 3 Multimode
829 Microplate Reader.
830
831 *Statistics*
832 Microscopy data sets were based on three biological replicates. One replicate includes per
833 time point the average of 14 - 15 images analyzed (with exception of Figure 4, which includes 14 – 35
834 analyzed cells per replicate and time point). For the infection assay, data sets were based on three
835 biological replicates. One biological replicate is the average of three technical replicates. Data was
836 tested for significance with a two-tailed, unpaired student's *t*-test with significance * = $p < 0.05$,
837 ** = $p < 0.01$ and *** = $p < 0.001$.
838
839
840 **Acknowledgement**
841 LF and TL were funded by the Deutsche Forschungsgemeinschaft (DFG, German Research Foundation),
842 Projektnummer 322863883 (LF and TL) and Projektnummer 270976260 (TL).
843
844
845 **References**
846 **Baker TS**, Newcomb WW, Olson NH, Cowsert LM, Olson C, Brown JC. 1991. Structures of bovine and
847 human papillomaviruses. Analysis by cryoelectron microscopy and three-dimensional image
848 reconstruction. *Biophysical journal* **60**:1445–1456. doi: 10.1016/S0006-3495(91)82181-6.
849 **Ballut L**, Sapay N, Chautard E, Imberty A, Ricard-Blum S. 2013. Mapping of heparin/heparan sulfate
850 binding sites on αvβ3 integrin by molecular docking. *Journal of molecular recognition : JMR* **26**:76–
851 85. doi: 10.1002/jmr.2250.

852 **Becker M**, Greune L, Schmidt MA, Schelhaas M. 2018. Extracellular Conformational Changes in the
853 Capsid of Human Papillomaviruses Contribute to Asynchronous Uptake into Host Cells. *Journal of*
854 *virology* **92**. doi: 10.1128/jvi.02106-17.
855 **Bienkowska-Haba M**, Luszczek W, Myers JE, Keiffer TR, DiGiuseppe S, Polk P, Bodily JM, Scott RS,
856 Sapp M. 2018. A new cell culture model to genetically dissect the complete human papillomavirus
857 life cycle. *PLoS Pathogens* **14**:e1006846. doi: 10.1371/journal.ppat.1006846.
858 **Bienkowska-Haba M**, Patel HD, Sapp M. 2009. Target cell cyclophilins facilitate human
859 papillomavirus type 16 infection. *PLoS Pathogens* **5**:e1000524. doi: 10.1371/journal.ppat.1000524.
860 **Bruening J**, Lasswitz L, Banse P, Kahl S, Marinach C, Vondran FW, Kaderali L, Silvie O, Pietschmann T,
861 Meissner F, Gerold G. 2018. Hepatitis C virus enters liver cells using the CD81 receptor complex
862 proteins calpain-5 and CBLB. *PLoS Pathogens* **14**:e1007111. doi: 10.1371/journal.ppat.1007111.
863 **Buck CB**, Pastrana DV, Lowy DR, Schiller JT. 2004. Efficient intracellular assembly of papillomaviral
864 vectors. *Journal of virology* **78**:751–757. doi: 10.1128/jvi.78.2.751-757.2004.
865 **Bugatti A**, Zani A, Bardelli M, Giovanetti M, Ravelli C, Ciccozzi M, Caruso A, Caccuri F. 2025. Heparan
866 sulfate proteoglycans remodel SARS-CoV-2 spike conformation to allow integrin interaction and
867 infection of endothelial cells. *Frontiers in cellular and infection microbiology* **15**:1552116.
868 doi: 10.3389/fcimb.2025.1552116.
869 **Cagno V**, Tseligka ED, Jones ST, Tapparel C. 2019. Heparan Sulfate Proteoglycans and Viral
870 Attachment: True Receptors or Adaptation Bias? *Viruses* **11**. doi: 10.3390/v11070596.
871 **Cerqueira C**, Samperio Ventayol P, Vogeley C, Schelhaas M. 2015. Kallikrein-8 Proteolytically
872 Processes Human Papillomaviruses in the Extracellular Space To Facilitate Entry into Host Cells.
873 *Journal of virology* **89**:7038–7052. doi: 10.1128/JVI.00234-15.
874 **Chang K**, Baginski J, Hassan SF, Volin M, Shukla D, Tiwari V. 2016. Filopodia and Viruses: An Analysis
875 of Membrane Processes in Entry Mechanisms. *Frontiers in microbiology* **7**:300.
876 doi: 10.3389/fmicb.2016.00300.
877 **Christiansen IK**, Sandve GK, Schmitz M, Dürst M, Hovig E. 2015. Transcriptionally active regions are
878 the preferred targets for chromosomal HPV integration in cervical carcinogenesis. *PloS one*
879 **10**:e0119566. doi: 10.1371/journal.pone.0119566.
880 **Clausen TM**, Sandoval DR, Spliid CB, Pihl J, Perrett HR, Painter CD, Narayanan A, Majowicz SA, Kwong
881 EM, McVicar RN, Thacker BE, Glass CA, Yang Z, Torres JL, Golden GJ, Bartels PL, Porell RN,
882 Garretson AF, Laubach L, Feldman J, Yin X, Pu Y, Hauser BM, Caradonna TM, Kellman BP, Martino
883 C, Gordts PLSM, Chanda SK, Schmidt AG, Godula K, Leibel SL, Jose J, Corbett KD, Ward AB, Carlin
884 AF, Esko JD. 2020. SARS-CoV-2 Infection Depends on Cellular Heparan Sulfate and ACE2. *Cell*
885 **183**:1043-1057.e15. doi: 10.1016/j.cell.2020.09.033.
886 **Cowin AJ**, Adams D, Geary SM, Wright MD, Jones JCR, Ashman LK. 2006. Wound healing is defective
887 in mice lacking tetraspanin CD151. *The Journal of investigative dermatology* **126**:680–689.
888 doi: 10.1038/sj.jid.5700142.
889 **Culp TD**, Budgeon LR, Marinkovich MP, Meneguzzi G, Christensen ND. 2006. Keratinocyte-secreted
890 laminin 5 can function as a transient receptor for human papillomaviruses by binding virions and
891 transferring them to adjacent cells. *Journal of virology* **80**:8940–8950. doi: 10.1128/JVI.00724-06.
892 **Dasgupta J**, Bienkowska-Haba M, Ortega ME, Patel HD, Bodevin S, Spillmann D, Bishop B, Sapp M,
893 Chen XS. 2011. Structural basis of oligosaccharide receptor recognition by human papillomavirus.
894 *The Journal of biological chemistry* **286**:2617–2624. doi: 10.1074/jbc.m110.160184.
895 **David G**, Bai XM, van der Schueren B, Cassiman JJ, van den Berghe H. 1992. Developmental changes
896 in heparan sulfate expression: in situ detection with mAbs. *The Journal of cell biology* **119**:961–
897 975. doi: 10.1083/jcb.119.4.961.

898 **Day PM**, Gambhira R, Roden RBS, Lowy DR, Schiller JT. 2008. Mechanisms of human papillomavirus
899 type 16 neutralization by l2 cross-neutralizing and l1 type-specific antibodies. *Journal of virology*
900 **82**:4638–4646. doi: 10.1128/JVI.00143-08.
901 **Day PM**, Schelhaas M. 2014. Concepts of papillomavirus entry into host cells. *Current opinion in*
902 *virology* **4**:24–31. doi: 10.1016/j.coviro.2013.11.002.
903 **Day PM**, Schiller JT. 2009. The role of furin in papillomavirus infection. *Future microbiology* **4**:1255–
904 1262. doi: 10.2217/fmb.09.86.
905 **Doorbar J**, Quint W, Banks L, Bravo IG, Stoler M, Broker TR, Stanley MA. 2012. The biology and life-
906 cycle of human papillomaviruses. *Vaccine* **30 Suppl 5**:F55-70. doi: 10.1016/j.vaccine.2012.06.083.
907 **Dziduszko A**, Ozbun MA. 2013. Annexin A2 and S100A10 regulate human papillomavirus type 16
908 entry and intracellular trafficking in human keratinocytes. *Journal of virology* **87**:7502–7515.
909 doi: 10.1128/JVI.00519-13.
910 **Earnest JT**, Hantak MP, Park J-E, Gallagher T. 2015. Coronavirus and influenza virus proteolytic
911 priming takes place in tetraspanin-enriched membrane microdomains. *Journal of virology*
912 **89**:6093–6104. doi: 10.1128/JVI.00543-15.
913 **Evander M**, Frazer IH, Payne E, Qi YM, Hengst K, McMillan NA. 1997. Identification of the alpha6
914 integrin as a candidate receptor for papillomaviruses. *Journal of virology* **71**:2449–2456.
915 doi: 10.1128/JVI.71.3.2449-2456.1997.
916 **Feng Y**, van Bodegraven D, Kádek A, L B Munguira I, Soria-Martinez L, Nentwich S, Saha S, Chardon F,
917 Kavan D, Uetrecht C, Schelhaas M, Roos WH. 2024. Glycan-induced structural activation softens
918 the human papillomavirus capsid for entry through reduction of intercapsomere flexibility. *Nature*
919 *communications* **15**:10076. doi: 10.1038/s41467-024-54373-0.
920 **Finke J**, Mikuličić S, Loster A-L, Gawlitza A, Florin L, Lang T. 2020. Anatomy of a viral entry platform
921 differentially functionalized by integrins α3 and α6. *Scientific reports* **10**:5356.
922 doi: 10.1038/s41598-020-62202-9.
923 **Florin L**, Lang T. 2018. Tetraspanin Assemblies in Virus Infection. *Frontiers in immunology* **9**:1140.
924 doi: 10.3389/fimmu.2018.01140.
925 **Galati L**, Chiantore MV, Marinaro M, Di Bonito P. 2024a. Human Oncogenic Viruses: Characteristics
926 and Prevention Strategies-Lessons Learned from Human Papillomaviruses. *Viruses* **16**.
927 doi: 10.3390/v16030416.
928 **Galati L**, Di Bonito P, Marinaro M, Chiantore MV, Gheit T. 2024b. HPV16 Phylogenetic Variants in
929 Anogenital and Head and Neck Cancers: State of the Art and Perspectives. *Viruses* **16**.
930 doi: 10.3390/v16060904.
931 **Gilson TD**, Gibson RT, Androphy EJ. 2020. Optimization of human papillomavirus-based pseudovirus
932 techniques for efficient gene transfer. *Scientific reports* **10**:15517. doi: 10.1038/s41598-020-
933 72027-1.
934 **Giroglou T**, Florin L, Schäfer F, Streeck RE, Sapp M. 2001. Human papillomavirus infection requires
935 cell surface heparan sulfate. *Journal of virology* **75**:1565–1570. doi: 10.1128/JVI.75.3.1565-
936 1570.2001.
937 **Hantak MP**, Qing E, Earnest JT, Gallagher T. 2019. Tetraspanins: Architects of Viral Entry and Exit
938 Platforms. *Journal of virology* **93**. doi: 10.1128/JVI.01429-17.
939 **Hemler ME**. 2005. Tetraspanin functions and associated microdomains. *Nature reviews. Molecular*
940 *cell biology* **6**:801–811. doi: 10.1038/nrm1736.
941 **Heuser J**. 2000. The production of 'cell cortices' for light and electron microscopy. *Traffic*
942 *(Copenhagen, Denmark)* **1**:545–552. doi: 10.1034/j.1600-0854.2000.010704.x.
943 **Hochdorfer D**, Florin L, Sinzger C, Lieber D. 2016. Tetraspanin CD151 Promotes Initial Events in
944 Human Cytomegalovirus Infection. *Journal of virology* **90**:6430–6442. doi: 10.1128/jvi.00145-16.

945 **Homsi Y**, Schloetel J-G, Scheffer KD, Schmidt TH, Destainville N, Florin L, Lang T. 2014. The
946 extracellular δ-domain is essential for the formation of CD81 tetraspanin webs. *Biophysical journal*
947 **107**:100–113. doi: 10.1016/j.bpj.2014.05.028.
948 **Jamieson RR**, Stasiak SE, Polio SR, Augspurg RD, McCormick CA, Ruberti JW, Parameswaran H. 2021.
949 Stiffening of the extracellular matrix is a sufficient condition for airway hyperreactivity. *Journal of*
950 *applied physiology (Bethesda, Md. : 1985)* **130**:1635–1645. doi: 10.1152/japplphysiol.00554.2020.
951 **Joyce JG**, Tung JS, Przysiecki CT, Cook JC, Lehman ED, Sands JA, Jansen KU, Keller PM. 1999. The L1
952 major capsid protein of human papillomavirus type 11 recombinant virus-like particles interacts
953 with heparin and cell-surface glycosaminoglycans on human keratinocytes. *The Journal of*
954 *biological chemistry* **274**:5810–5822. doi: 10.1074/jbc.274.9.5810.
955 **Kines RC**, Thompson CD, Lowy DR, Schiller JT, Day PM. 2009. The initial steps leading to
956 papillomavirus infection occur on the basement membrane prior to cell surface binding.
957 *Proceedings of the National Academy of Sciences of the United States of America* **106**:20458–
958 20463. doi: 10.1073/pnas.0908502106.
959 **Knappe M**, Bodevin S, Selinka H-C, Spillmann D, Streeck RE, Chen XS, Lindahl U, Sapp M. 2007.
960 Surface-exposed amino acid residues of HPV16 L1 protein mediating interaction with cell surface
961 heparan sulfate. *The Journal of biological chemistry* **282**:27913–27922.
962 doi: 10.1074/jbc.m705127200.
963 **Martel C** de, Plummer M, Vignat J, Franceschi S. 2017. Worldwide burden of cancer attributable to
964 HPV by site, country and HPV type. *International journal of cancer* **141**:664–670.
965 doi: 10.1002/ijc.30716.
966 **Mertens G**, van der Schueren B, van den Berghe H, David G. 1996. Heparan sulfate expression in
967 polarized epithelial cells: the apical sorting of glypican (GPI-anchored proteoglycan) is inversely
968 related to its heparan sulfate content. *The Journal of cell biology* **132**:487–497.
969 doi: 10.1083/jcb.132.3.487.
970 **Mikuličić S**, Finke J, Boukhallouk F, Wüstenhagen E, Sons D, Homsi Y, Reiss K, Lang T, Florin L. 2019.
971 ADAM17-dependent signaling is required for oncogenic human papillomavirus entry platform
972 assembly. *eLife* **8**. doi: 10.7554/eLife.44345.
973 **Mikuličić S**, Massenberg A, Döring T, Brandenburg K, Lang T, Florin L. 2025. HSPG-binding peptide
974 Pep19-2.5 is a potent inhibitor of HPV16 infection. *Antimicrobial agents and chemotherapy*
975 **69**:e0157524. doi: 10.1128/aac.01575-24.
976 **Mikuličić S**, Strunk J, Florin L. 2021. HPV16 Entry into Epithelial Cells: Running a Gauntlet. *Viruses* **13**.
977 doi: 10.3390/v13122460.
978 **Miladinova E**, Lilkova E, Krachmarova E, Malinova K, Petkov P, Ilieva N, Nacheva G, Litov L. 2022.
979 Heparan Sulfate Facilitates Binding of hIFNγ to Its Cell-Surface Receptor hIFNGR1. *International*
980 *journal of molecular sciences* **23**. doi: 10.3390/ijms23169415.
981 **Ozbun MA**. 2019. Extracellular events impacting human papillomavirus infections: Epithelial
982 wounding to cell signaling involved in virus entry. *Papillomavirus research (Amsterdam,*
983 *Netherlands)* **7**:188–192. doi: 10.1016/j.pvr.2019.04.009.
984 **Ozbun MA**, Campos SK. 2021. The long and winding road: human papillomavirus entry and
985 subcellular trafficking. *Current opinion in virology* **50**:76–86. doi: 10.1016/j.coviro.2021.07.010.
986 **Pellegrini L**. 2001. Role of heparan sulfate in fibroblast growth factor signalling: a structural view.
987 *Current opinion in structural biology* **11**:629–634. doi: 10.1016/s0959-440x(00)00258-x.
988 **Peng GE**, Wilson SR, Weiner OD. 2011. A pharmacological cocktail for arresting actin dynamics in
989 living cells. *Molecular biology of the cell* **22**:3986–3994. doi: 10.1091/mbc.E11-04-0379.
990 **Richards KF**, Bienkowska-Haba M, Dasgupta J, Chen XS, Sapp M. 2013. Multiple heparan sulfate
991 binding site engagements are required for the infectious entry of human papillomavirus type 16.
992 *Journal of virology* **87**:11426–11437. doi: 10.1128/jvi.01721-13.

993 **Richards KF**, Mukherjee S, Bienkowska-Haba M, Pang J, Sapp M. 2014. Human papillomavirus
994 species-specific interaction with the basement membrane-resident non-heparan sulfate receptor.
995 *Viruses* **6**:4856–4879. doi: 10.3390/v6124856.
996 **Richards RM**, Lowy DR, Schiller JT, Day PM. 2006. Cleavage of the papillomavirus minor capsid
997 protein, L2, at a furin consensus site is necessary for infection. *Proceedings of the National*
998 *Academy of Sciences of the United States of America* **103**:1522–1527.
999 doi: 10.1073/pnas.0508815103.
1000 **Rommel O**, Dillner J, Fligge C, Bergsdorf C, Wang X, Selinka H-C, Sapp M. 2005. Heparan sulfate
1001 proteoglycans interact exclusively with conformationally intact HPV L1 assemblies: basis for a
1002 virus-like particle ELISA. *Journal of medical virology* **75**:114–121. doi: 10.1002/jmv.20245.
1003 **Scheffer KD**, Gawlitza A, Spoden GA, Zhang XA, Lambert C, Berditchevski F, Florin L. 2013.
1004 Tetraspanin CD151 mediates papillomavirus type 16 endocytosis. *Journal of virology* **87**:3435–
1005 3446. doi: 10.1128/JVI.02906-12.
1006 **Schelhaas M**, Ewers H, Rajamäki M-L, Day PM, Schiller JT, Helenius A. 2008. Human papillomavirus
1007 type 16 entry: retrograde cell surface transport along actin-rich protrusions. *PLoS Pathogens*
1008 **4**:e1000148. doi: 10.1371/journal.ppat.1000148.
1009 **Schelhaas M**, Shah B, Holzer M, Blattmann P, Kühling L, Day PM, Schiller JT, Helenius A. 2012. Entry
1010 of human papillomavirus type 16 by actin-dependent, clathrin- and lipid raft-independent
1011 endocytosis. *PLoS Pathogens* **8**:e1002657. doi: 10.1371/journal.ppat.1002657.
1012 **Schiller JT**, Day PM, Kines RC. 2010. Current understanding of the mechanism of HPV infection.
1013 *Gynecologic oncology* **118**:S12-7. doi: 10.1016/j.ygyno.2010.04.004.
1014 **Schindelin J**, Arganda-Carreras I, Frise E, Kaynig V, Longair M, Pietzsch T, Preibisch S, Rueden C,
1015 Saalfeld S, Schmid B, Tinevez J-Y, White DJ, Hartenstein V, Eliceiri K, Tomancak P, Cardona A. 2012.
1016 Fiji: an open-source platform for biological-image analysis. *Nature methods* **9**:676–682.
1017 doi: 10.1038/nmeth.2019.
1018 **Schmidt SC**, Massenberg A, Homsi Y, Sons D, Lang T. 2024. Microscopic clusters feature the
1019 composition of biochemical tetraspanin-assemblies and constitute building-blocks of tetraspanin
1020 enriched domains. *Scientific reports* **14**:2093. doi: 10.1038/s41598-024-52615-1.
1021 **Selinka H-C**, Florin L, Patel HD, Freitag K, Schmidtke M, Makarov VA, Sapp M. 2007. Inhibition of
1022 transfer to secondary receptors by heparan sulfate-binding drug or antibody induces
1023 noninfectious uptake of human papillomavirus. *Journal of virology* **81**:10970–10980.
1024 doi: 10.1128/jvi.00998-07.
1025 **Selinka H-C**, Giroglou T, Sapp M. 2002. Analysis of the infectious entry pathway of human
1026 papillomavirus type 33 pseudovirions. *Virology* **299**:279–287. doi: 10.1006/viro.2001.1493.
1027 **Smith JL**, Lidke DS, Ozbun MA. 2008. Virus activated filopodia promote human papillomavirus type
1028 31 uptake from the extracellular matrix. *Virology* **381**:16–21. doi: 10.1016/j.virol.2008.08.040.
1029 **Spoden G**, Freitag K, Husmann M, Boller K, Sapp M, Lambert C, Florin L. 2008. Clathrin- and caveolin-
1030 independent entry of human papillomavirus type 16--involvement of tetraspanin-enriched
1031 microdomains (TEMs). *PloS one* **3**:e3313. doi: 10.1371/journal.pone.0003313.
1032 **Spoden G**, Kühling L, Cordes N, Frenzel B, Sapp M, Boller K, Florin L, Schelhaas M. 2013. Human
1033 papillomavirus types 16, 18, and 31 share similar endocytic requirements for entry. *Journal of*
1034 *virology* **87**:7765–7773. doi: 10.1128/jvi.00370-13.
1035 **Spoden GA**, Besold K, Krauter S, Plachter B, Hanik N, Kilbinger AFM, Lambert C, Florin L. 2012.
1036 Polyethylenimine is a strong inhibitor of human papillomavirus and cytomegalovirus infection.
1037 *Antimicrobial agents and chemotherapy* **56**:75–82. doi: 10.1128/aac.05147-11.
1038 **Sterk LM**, Geuijen CA, Oomen LC, Calafat J, Janssen H, Sonnenberg A. 2000. The tetraspan molecule
1039 CD151, a novel constituent of hemidesmosomes, associates with the integrin alpha6beta4 and

1040 may regulate the spatial organization of hemidesmosomes. *The Journal of cell biology* **149**:969–
1041 982. doi: 10.1083/jcb.149.4.969.
1042 **Surviladze Z**, Dziduszko A, Ozbun MA. 2012. Essential Roles for Soluble Virion-Associated Heparan
1043 Sulfonated Proteoglycans and Growth Factors in Human Papillomavirus Infections. *PLoS*
1044 *Pathogens* **8**:e1002519. doi: 10.1371/journal.ppat.1002519.
1045 **Surviladze Z**, Sterkand RT, Ozbun MA. 2015. Interaction of human papillomavirus type 16 particles
1046 with heparan sulfate and syndecan-1 molecules in the keratinocyte extracellular matrix plays an
1047 active role in infection. *The Journal of general virology* **96**:2232–2241. doi: 10.1099/vir.0.000147.
1048 **Tian J**, Li C, Li W. 2021. Entry of hepatitis B virus: going beyond NTCP to the nucleus. *Current opinion*
1049 *in virology* **50**:97–102. doi: 10.1016/j.coviro.2021.08.001.
1050 **Vasioukhin V**, Bauer C, Yin M, Fuchs E. 2000. Directed actin polymerization is the driving force for
1051 epithelial cell-cell adhesion. *Cell* **100**:209–219. doi: 10.1016/s0092-8674(00)81559-7.
1052 **Woodham AW**, Da Silva DM, Skeate JG, Raff AB, Ambroso MR, Brand HE, Isas JM, Langen R, Kast
1053 WM. 2012. The S100A10 subunit of the annexin A2 heterotetramer facilitates L2-mediated human
1054 papillomavirus infection. *PloS one* **7**:e43519. doi: 10.1371/journal.pone.0043519.
1055 **Wüstenhagen E**, Boukhallouk F, Negwer I, Rajalingam K, Stubenrauch F, Florin L. 2018. The Myb-
1056 related protein MYPOP is a novel intrinsic host restriction factor of oncogenic human
1057 papillomaviruses. *Oncogene* **37**:6275–6284. doi: 10.1038/s41388-018-0398-6.
1058 **Yokoyama H**, Sato K, Okudaira M, Morita C, Takahashi C, Suzuki D, Sakai H, Iwamoto Y. 1999. Serum
1059 and urinary concentrations of heparan sulfate in patients with diabetic nephropathy. *Kidney*
1060 *international* **56**:650–658. doi: 10.1046/j.1523-1755.1999.00591.x.
1061 **Yoon CS**, Kim KD, Park SN, Cheong SW. 2001. alpha(6) Integrin is the main receptor of human
1062 papillomavirus type 16 VLP. *Biochemical and biophysical research communications* **283**:668–673.
1063 doi: 10.1006/bbrc.2001.4838.
1064 **Zhang Q**, Tang W, Stancanelli E, Jung E, Syed Z, Pagadala V, Saidi L, Chen CZ, Gao P, Xu M, Pavlinov I,
1065 Li B, Huang W, Chen L, Liu J, Xie H, Zheng W, Ye Y. 2023. Host heparan sulfate promotes ACE2
1066 super-cluster assembly and enhances SARS-CoV-2-associated syncytium formation. *Nature*
1067 *communications* **14**:5777. doi: 10.1038/s41467-023-41453-w.
1068 **Zona L**, Lupberger J, Sidahmed-Adrar N, Thumann C, Harris HJ, Barnes A, Florentin J, Tawar RG, Xiao
1069 F, Turek M, Durand SC, Duong FHT, Heim MH, Cosset F-L, Hirsch I, Samuel D, Brino L, Zeisel MB, Le
1070 Naour F, McKeating JA, Baumert TF. 2013. HRas signal transduction promotes hepatitis C virus cell
1071 entry by triggering assembly of the host tetraspanin receptor complex. *Cell host & microbe*
1072 **13**:302–313. doi: 10.1016/j.chom.2013.02.006.
1073 **zur Hausen H**. 2009. The search for infectious causes of human cancers: where and why (Nobel
1074 lecture). *Angewandte Chemie (International ed. in English)* **48**:5798–5808.
1075 doi: 10.1002/anie.200901917.
1076

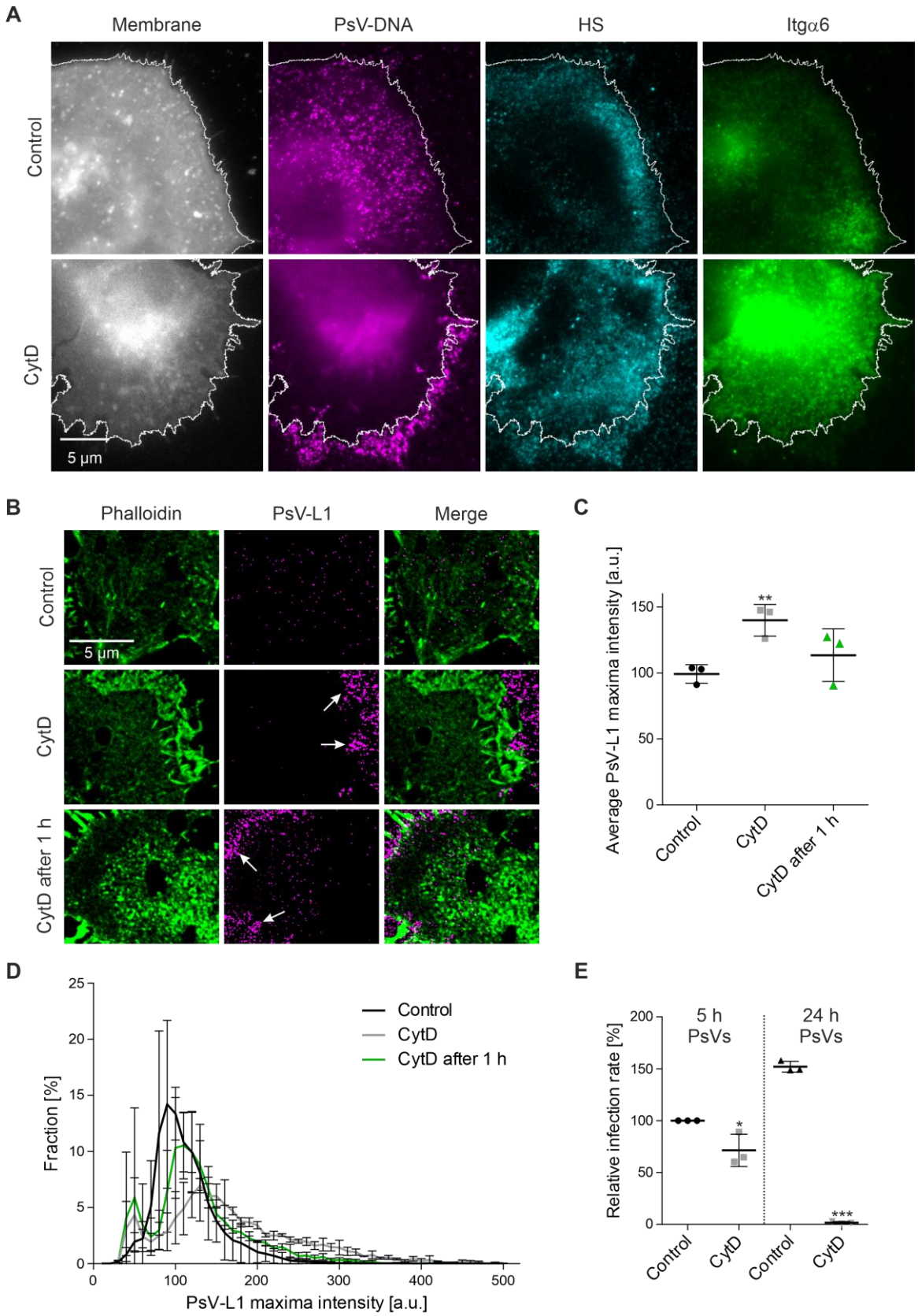

Figure 1. *CytD arrests PsV translocation from the ECM to the cell body.*
(A) In the absence (Control) or presence of 10 µg/ml CytD (CytD), HaCaT cells were incubated with PsVs at 37 °C for 5 h. Then, cells were fixed, washed and stained with the cell membrane dye TMA-DPH (gray lookup table (LUT)). PsVs (magenta LUT) were visualized through coupling a dye (6-FAM Azide) to the encapsidated plasmid by click-chemistry. Indirect immunolabeling was employed for

1083 staining of HS (AlexaFluor 594; cyan LUT) and Itgα6 (STARRED; green LUT). Imaging was realized with
1084 epi-fluorescence microscopy. White lines delineate the main cell body; lines were created with
1085 reference to the TMA-DPH membrane staining. (B) Same pre-treatment of cells as in (A), with an
1086 additional condition where CytD was added 1 h after the PsVs (CytD after 1 h). Prior to fixation,
1087 membrane sheets were generated and F-actin was stained with phalloidin coupled to iFluor488 (green
1088 LUT). The capsid protein L1 of the PsVs and CD151 were stained by immunofluorescence using primary
1089 antibodies in combination with AlexaFluor 594-labelled (L1, magenta LUT) and STAR RED-labelled
1090 (CD151, not shown in this figure for clarity reasons) secondary antibodies. Images of phalloidin and L1
1091 staining were acquired in the confocal and STED mode of a STED microscope, respectively. Arrows in
1092 the PsV-L1 images point towards accumulated PsVs that after CytD are more frequently observed than
1093 in the control (see text). (C) Analysis of images as shown in (B) using ROIs covering the whole image.
1094 PsV maxima were detected and their intensities were quantified in a circular 125 nm diameter region
1095 of interest (ROI), followed by background correction. Values are given as means ± SD (n = 3; one
1096 biological replicate includes per condition the average of 14 - 15 analyzed membranes (intensity values
1097 of one membrane sheet were averaged) with altogether at least 1000 maxima intensity values). (D)
1098 PsV maxima intensity distribution of the data in (C). The fraction of PsVs, expressed in percent, is
1099 plotted as histogram (10 a.u. bins) against the maxima intensity. Values are given as means ± SD (n =
1100 3). (E) HaCaT cells were treated either for 5 h or 24 h with PsVs, together without (Control) or with
1101 10 µg/ml CytD (CytD). In case of the 5 h incubation, after removal of the PsVs/CytD cells were
1102 incubated for another 19 h in medium (in total 24 h). After a total of 24 h incubation, the luciferase
1103 activity of lysed cells was measured, yielding the infection rate that was normalized to LDH, resulting
1104 in the normalized infection rate. The normalized infection rate was further related to the mean
1105 normalized infection rate of the 5 h control, set to 100%, yielding the relative infection rate. Values
1106 are given as means ± SD (n = 3 biological replicates; the value of one biological replicate is the average
1107 of three technical replicates). (C) and (E). Statistical differences between Control and CytD was
1108 analyzed by using the two-tailed, unpaired student's *t*-test (n = 3, for details see methods). a.u.,
1109 arbitrary units.

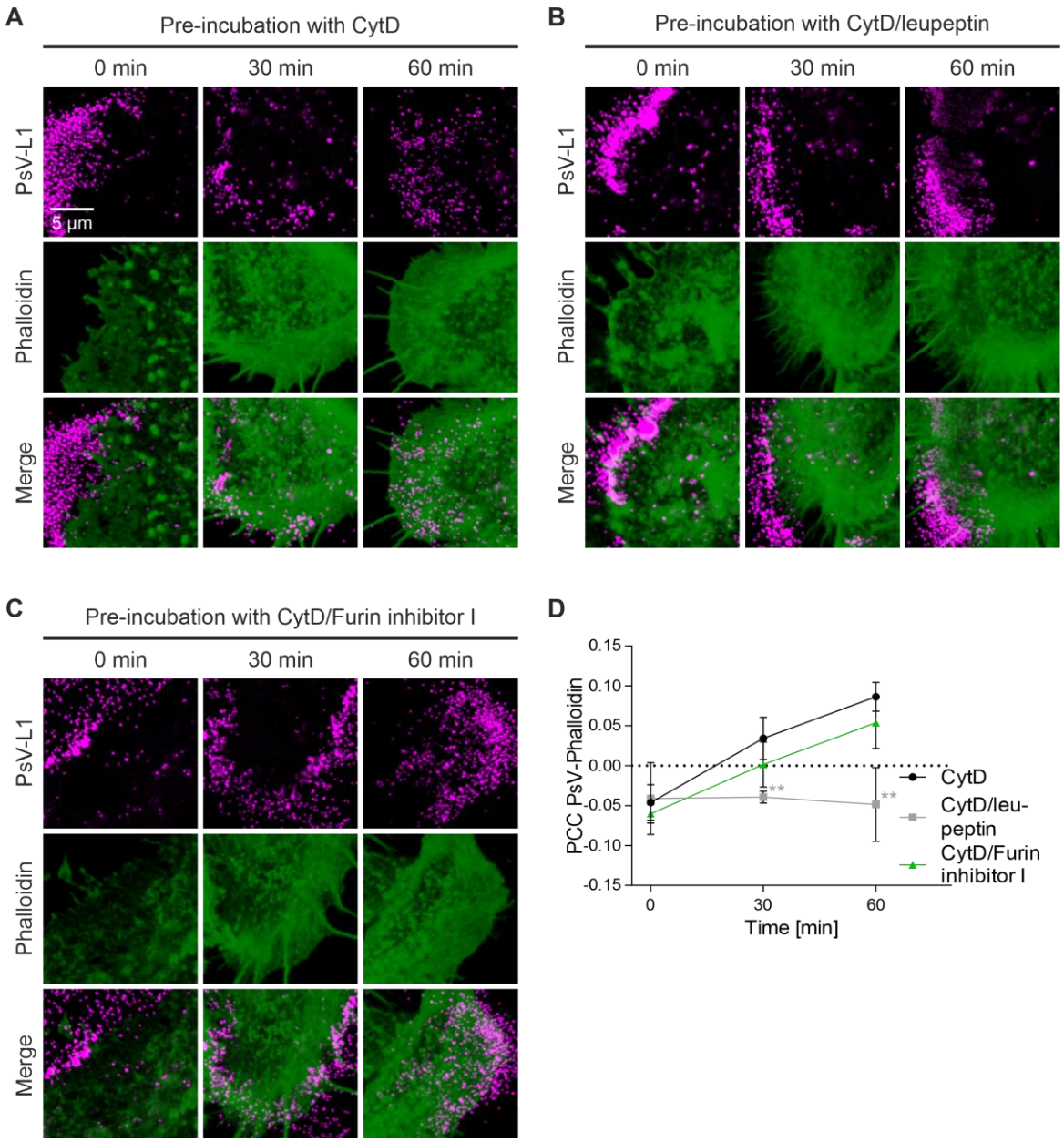

Figure 2. *Transfer of PsVs from the ECM to the cell body requires PsV priming.*
HaCaT cells were pre-incubated for 5 h at 37 °C with PsVs, in the presence of (A) 10 µg/ml CytD (CytD), (B) 10 µg/ml CytD and 100 µM leupeptin (CytD/leupeptin), or (C) 10 µg/ml CytD and 5 µM Furin inhibitor I (CytD/Furin inhibitor I). Afterwards, cells were washed and incubated without PsVs/inhibitors further for 0 min, 30 min or 60 min, before they were fixed and stained by indirect immunofluorescence for L1 (STAR GREEN, magenta LUT) and for F-actin by iFluor647-labelled phalloidin (green LUT). PsVs-L1 and F-actin staining were imaged in the confocal mode of a STED microscope. (D) For determination of the Pearson correlation coefficient (PCC) between PsV-L1 (magenta LUT) and Phalloidin (green LUT), we placed large ROIs onto the images that covered mainly the cell body but included parts of the cell periphery as well. The PCC was plotted over time. Values are given as means ± SD (n = 3 biological replicates). Statistical difference between CytD and CytD/inhibitors was analyzed by using the two-tailed, unpaired student's *t*-test (n = 3, for details see methods).

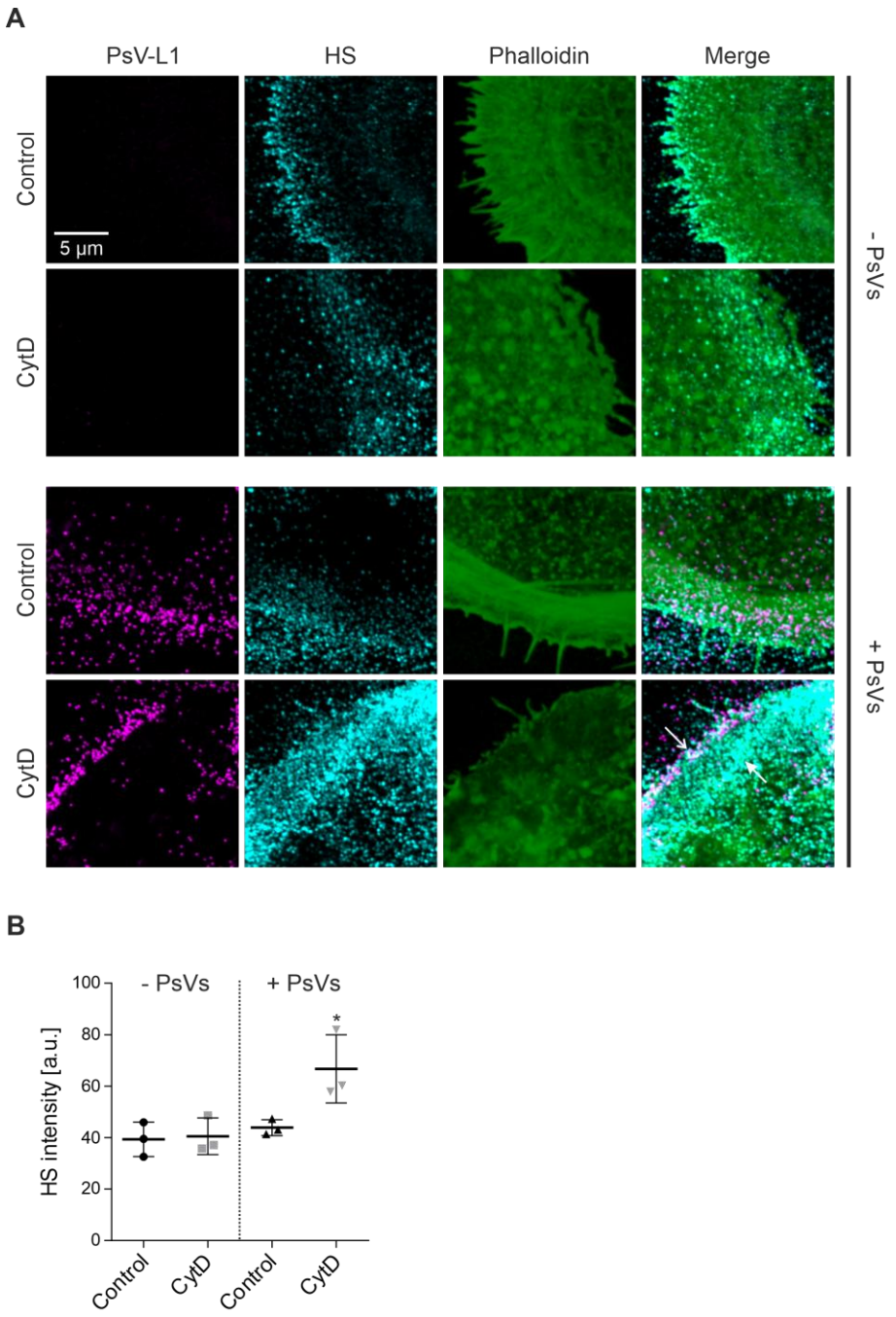

Figure 3. *Increased HS intensity after incubation with PsVs and CytD.*
(A) HaCaT cells were incubated without (top) and with (bottom) PsVs at 37 °C for 5 h, in the absence (Control, upper panels) or presence of 10 µg/ml CytD (CytD, lower panels). Afterwards, cells were washed, fixed and stained. Immunofluorescence was used for L1 (STAR GREEN; magenta LUT) and for HS (AlexaFluor 594; cyan LUT). F-actin was stained by iFluor647-labelled phalloidin (green LUT). PsVs-L1, HS and F-actin staining were imaged in the confocal mode of a STED microscope. The open arrow marks a region where PsVs overlap with HS. The closed arrow marks a region devoid of PsVs showing strong HS staining. (B) For analysis of the mean HS intensity, we placed large ROIs onto the images covering mainly the cell body but including parts of the cell periphery as well. Values are given as means ± SD (n = 3 biological replicates). Statistical differences between Control and CytD were analyzed by using the two-tailed, unpaired student's *t*-test (n = 3, for details see methods).

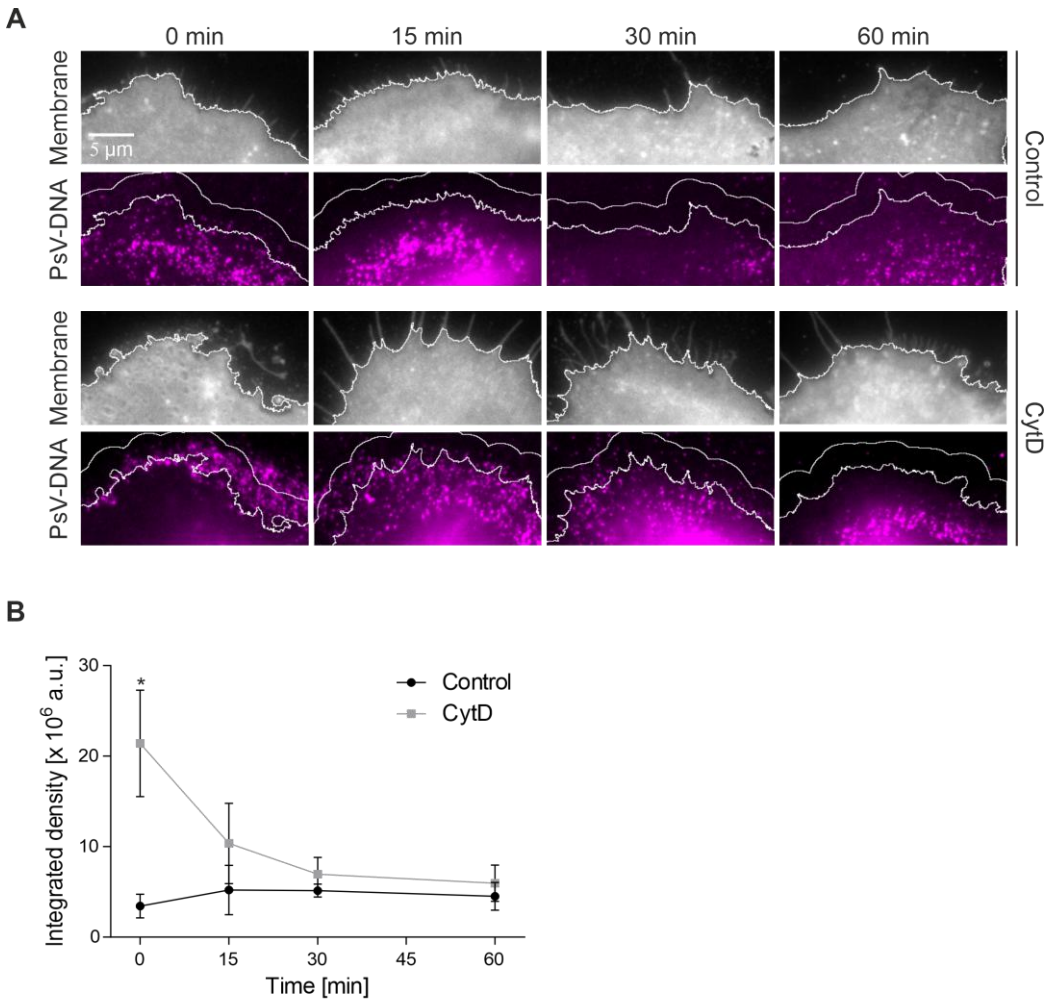

1137
1138 **Figure 4.** *Fast diminishment of accumulated PsVs at the cell periphery after removal of CytD.*
1139 (A) HaCaT cells were incubated with PsVs at 37 °C for 5 h, in the absence (Control) or presence of
1140 10 µg/ml CytD (CytD). Then, cells were washed and incubated for the indicated time periods without
1141 PsVs/CytD, before they were fixed and stained as in Figure 1 (t = 0 min is identical to Figure 1A; for
1142 clarity we show only the membrane (gray LUT; images are shown at different settings of brightness
1143 and contrast) and the PsV-DNA staining (magenta LUT; images are shown at the same settings of
1144 brightness and contrast). The white lines in the membrane images delineate the cell body from the
1145 periphery. They were created with reference to the membrane staining (for details see methods).
1146 Using the cell body delineation as starting point, an up to 30-pixel broad area was created (PsV
1147 channel, magenta LUT; see area enclosed by the smoother white lines and the cell body delineation
1148 lines). The area enclosed by the two white lines defines the cell periphery. (B) The PsV-DNA signal of
1149 the periphery was quantified as integrated density, background corrected, and plotted over time.
1150 Values are given as means ± SD (n = 3 biological replicates). The statistical difference between the
1151 same time points of Control and CytD were analyzed by using the two-tailed, unpaired student's *t*-test
1152 (n = 3, for details see methods).

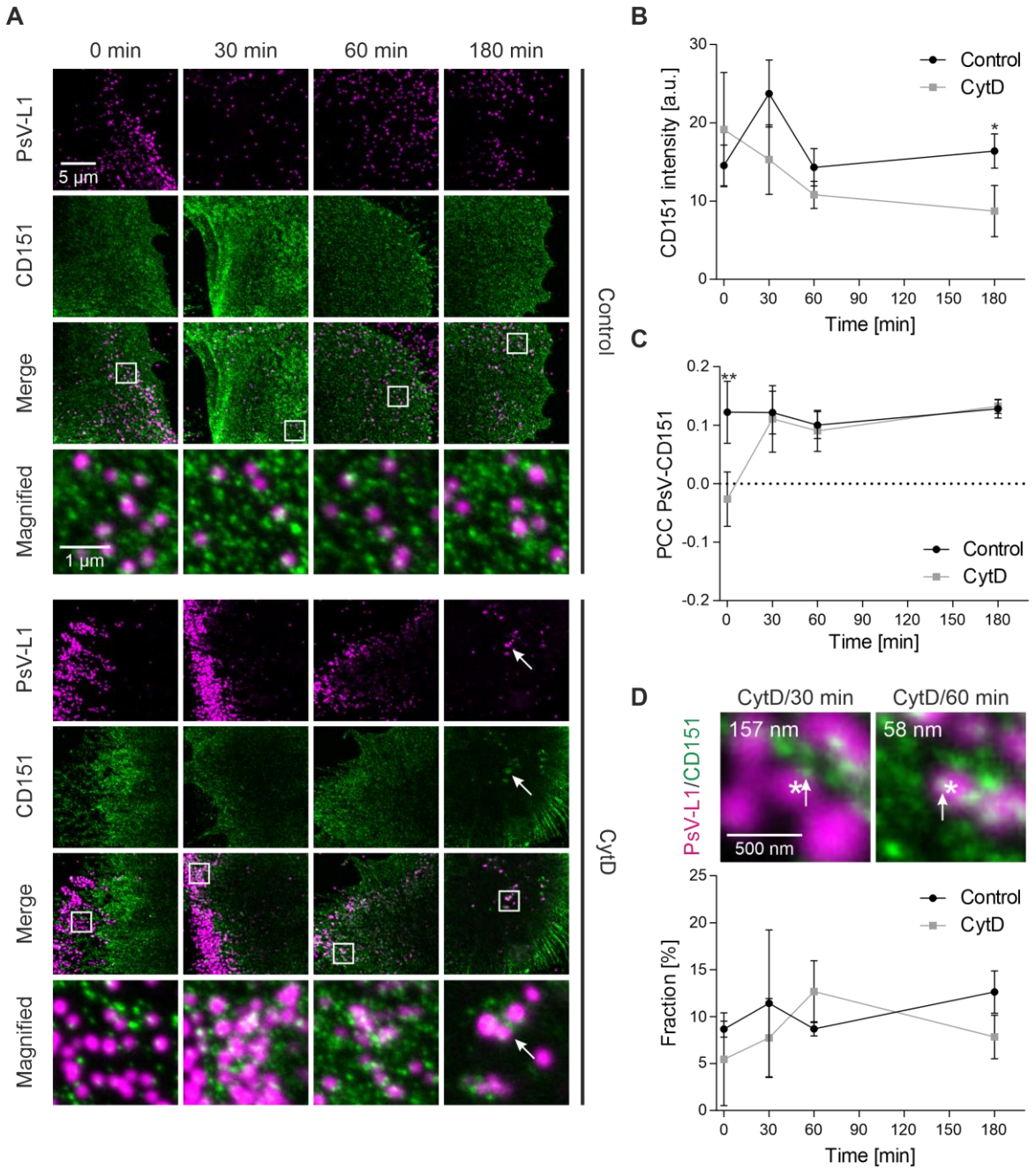

Figure 5. *Association between PsVs and CD151 is an early event in the infection cascade.*
(A) HaCaT cells were incubated with PsVs at 37 °C for 5 h, in the absence (Control, upper panels) or presence of 10 µg/ml CytD (CytD, lower panels). Afterwards, cells were washed and incubated without PsVs/CytD further for 0 min, 30 min, 60 min or 180 min, before they were fixed and stained by indirect immunofluorescence for L1 (STAR GREEN; magenta LUT) and for CD151 (AlexaFluor 594; green LUT), and for F-actin by iFluor647-labelled phalloidin (here not shown for clarity, please see Supplementary Figure 3 for F-actin illustrating the variability of filopodia after CytD treatment). The bottom rows show magnified views of the merged images from the regions marked by the white boxes. PsV-L1 and F-actin staining were imaged in the confocal and CD151 staining in the STED mode of a STED microscope, respectively. Therefore, compared to CD151, the PsVs are less resolved and also appear much larger than their real physical size (see magnified views). CytD/180 min, arrows mark presumably endocytic structures that formed in the central cell body region (for more examples see Supplementary Figure 5). For analysis, we placed large ROIs onto the images that covered mainly the cell body but included

1167 parts of the cell periphery as well (for an example ROI see Supplementary Figure 6A). (B) The mean
1168 CD151 intensity was measured and plotted over time. (C) The PCC between PsV-L1 (magenta LUT) and
1169 CD151 (green LUT) was calculated and plotted over time. (D) The fraction of PsVs (in percent) that
1170 have a distance to the next neighbored CD151 maximum ≤ 80 nm, which we define as closely
1171 associated, is plotted over time. Please note that the values in (D) were corrected for random
1172 background association (for details see Supplementary Figure 7). Two examples of PsVs (each marked
1173 by an asterisk) from the CytD/30 min (left) and CytD/60 min (right) conditions are shown. The value in
1174 the upper left states the shortest distance between the PsV and the next nearest CD151 maximum
1175 (marked by an arrow) in nm. Values are given as means ± SD (n = 3 biological replicates). Statistical
1176 differences between the same time points of Control and CytD were analyzed by using the two-tailed,
1177 unpaired student's *t*-test (n = 3, for details see methods).

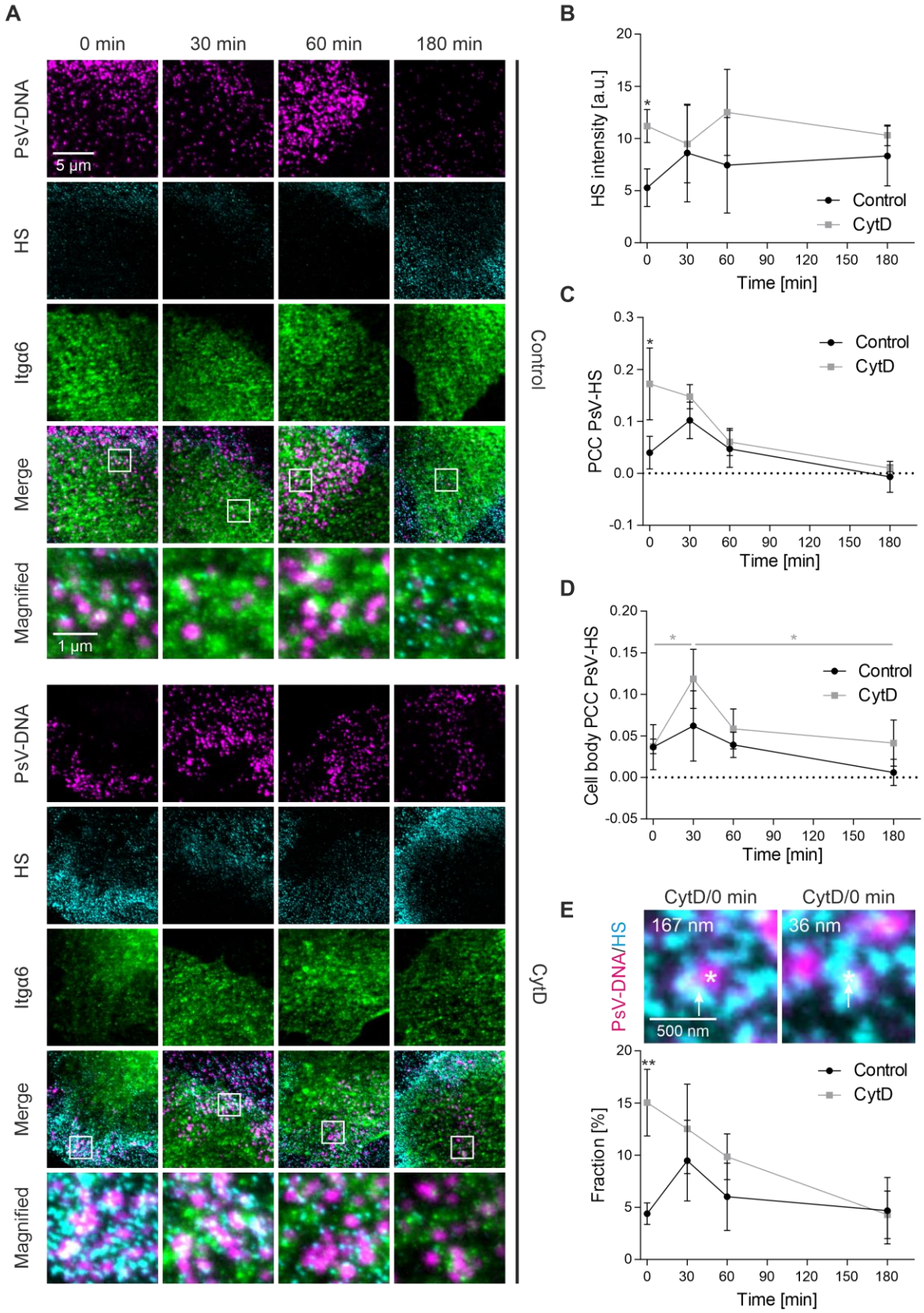

Figure 6. *Association between PsVs and HS.*
(A) HaCaT cells were incubated with PsVs at 37 °C for 5 h, in the absence (Control, upper panels) or presence of 10 µg/ml CytD (CytD, lower panels). Afterwards, cells were washed and incubated without

1182 PsVs/CytD further for up to 180 min, before they were fixed and stained. PsVs (magenta LUT) were
1183 visualized by click-chemistry (6-FAM Azide) and indirect immunolabeling was used for HS (AlexaFluor
1184 594; cyan LUT) and for Itgα6 (STAR RED; green LUT). The bottom rows show magnified views of the
1185 white boxes in the merged images. PsV-DNA staining was imaged in the confocal and HS and Itgα6
1186 staining in the STED mode of a STED microscope. For analysis, we placed large ROIs onto the images
1187 that covered mainly the cell body but included parts of the cell periphery as well (see example in
1188 Supplementary Figure 8A). For (D), smaller ROIs covering only the cell body region were used. (B) The
1189 mean HS intensity plotted over time. (C) The PCC between PsV-DNA (magenta LUT) and HS (cyan LUT)
1190 over time. (D) The PCC between PsV-DNA (magenta LUT) and HS (cyan LUT) in the region of the cell
1191 body over time. (E) The fraction of PsVs (in percent) closely associating with HS (distance ≤ 80 nm)
1192 plotted over time (for background correction see Supplementary Figure 9). Two examples of PsVs
1193 (each marked by an asterisk) from the CytD/0 min condition are shown. The value in the upper left
1194 corner states the shortest distance (in nm) between the marked PsV and its next nearest HS maximum
1195 (marked by an arrow). Values are given as means ± SD (n = 3 biological replicates). Using the two-
1196 tailed, unpaired student's *t*-test (n = 3 biological replicates), we analyzed in (B), (C) and (E) the
1197 statistical differences between the same time points of Control and CytD, and in (D) the difference
1198 between CytD/30 min and CytD/0 min or CytD/180 min (for details see methods).
1199

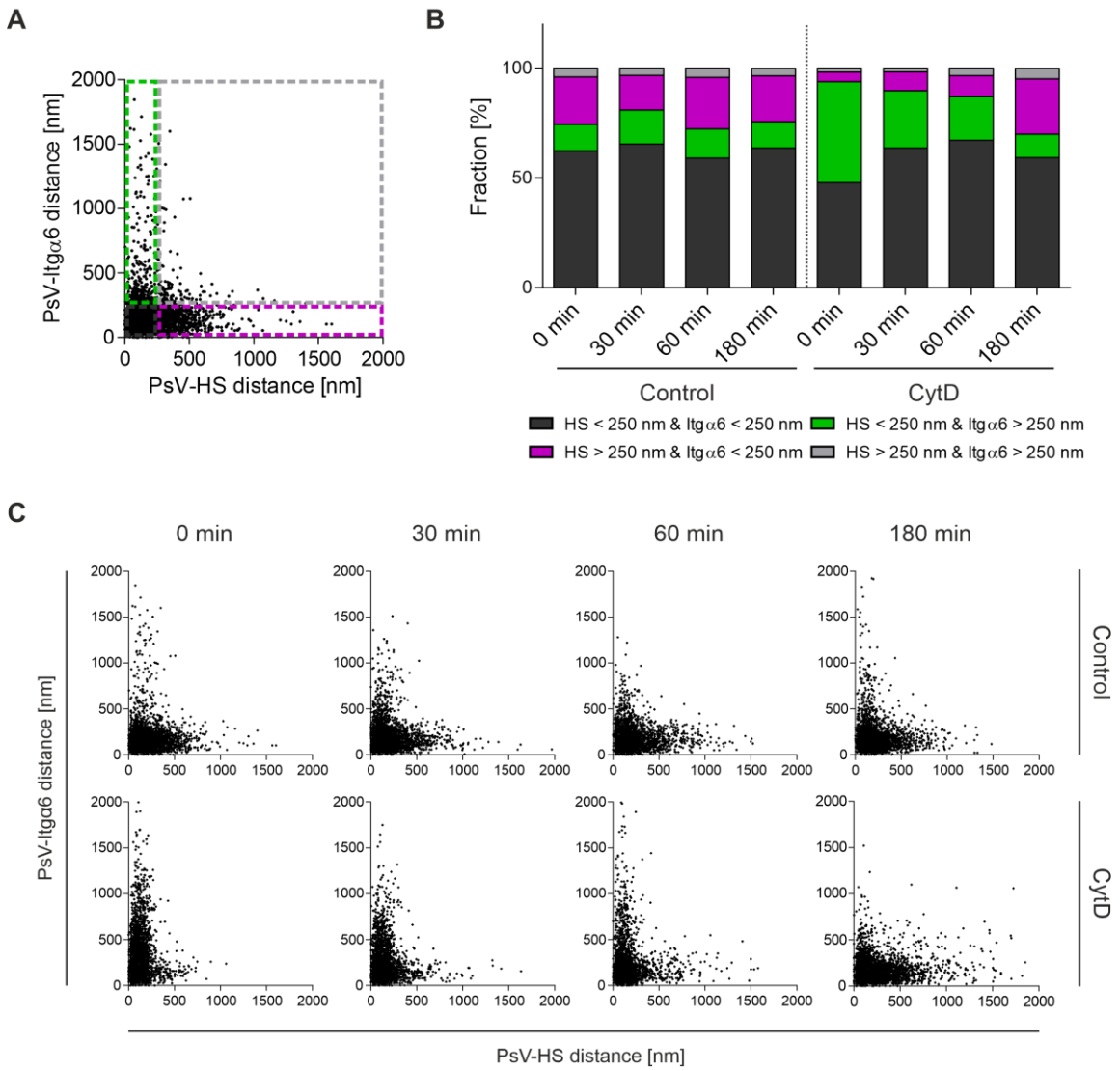

Figure 7. *PsV-Itgα6 and PsV-HS distances over time.*
(A) Definition of four PsV populations based on the PsV distances to Itgα6 and HS (the plot is taken from Control, 0 min and shown again in C). Dashed green rectangle, PsVs with a distance to HS < 250 nm and to Itgα6 > 250 nm. Dashed magenta rectangle, PsVs with a distance to HS > 250 nm and to Itgα6 < 250 nm. Dashed gray square, PsVs with a distance to HS > 250 nm and to Itgα6 > 250 nm. PsVs not included in the previous categories have a distance to HS < 250 nm and to Itgα6 < 250 nm (dashed black square). (B) From the PsVs analyzed in Figure 6, for the Control (left) and CytD (right) the PsV fraction size (in percent) of each population is illustrated. Shown are the means of three biological replicates. For means ± SD and statistical analysis see Supplementary Table 1. (C) For the Control (top) and CytD (bottom), for each PsV, we plotted the shortest distance to Itgα6 against the shortest distance to HS (pooling the three biological replicates; 3,043 – 4,080 PsVs per plot).

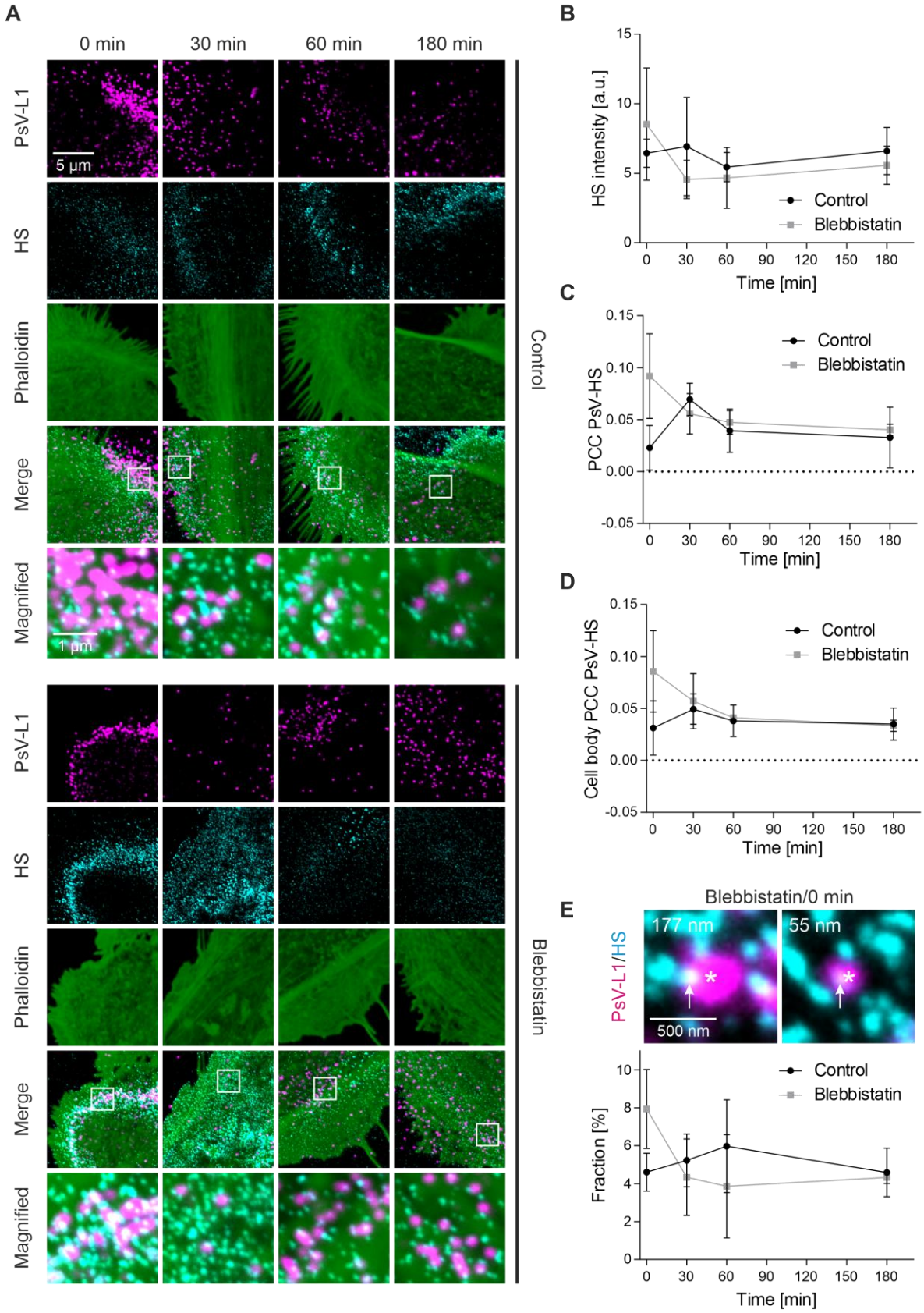

Figure 8. *Association between PsVs and HS after blebbistatin treatment.*
(A) HaCaT cells were incubated with PsVs at 37 °C for 5 h, in the absence (Control, upper panels) or presence of 30 µM blebbistatin (Blebbistatin, lower panels). Afterwards, cells were washed and

incubated without PsVs/blebbistatin further for up to 180 min, before they were fixed and stained. Immunofluorescence was used for L1 (STAR GREEN; magenta LUT) and HS (AlexaFluor 594; cyan LUT) staining. F-actin was stained by iFluor647-labelled phalloidin (green LUT). The bottom rows show magnified views of the white boxes in the merged images. PsVs and F-actin staining were imaged in the confocal and HS staining in the STED mode of a STED microscope. For analysis, we placed large ROIs onto the images that covered mainly the cell body but included parts of the cell periphery as well. For (D), smaller ROIs covering only the cell body region were used. (B) Mean HS intensity over time. (C) PCC between PsV-L1 (magenta LUT) and HS (cyan LUT) over time. (D) PCC between PsV-L1 (magenta LUT) and HS (cyan LUT) in the region of the cell body over time. (E) The fraction of PsVs (in percent) closely associating with HS (distance ≤ 80 nm) plotted over time (for background correction see Supplementary Figure 11). Two examples of PsVs (each marked by an asterisk) from the blebbistatin/0 min condition are shown. The value in the upper left states the shortest distance between the PsV and its next nearest HS maximum (marked by an arrow) in nm. Values are given as means ± SD (n = 3 biological replicates). Statistical differences between the same time points of Control and Blebbistatin were analyzed by using the two-tailed, unpaired student's *t*-test (n = 3), but the analysis yielded no p-values below 0.05.

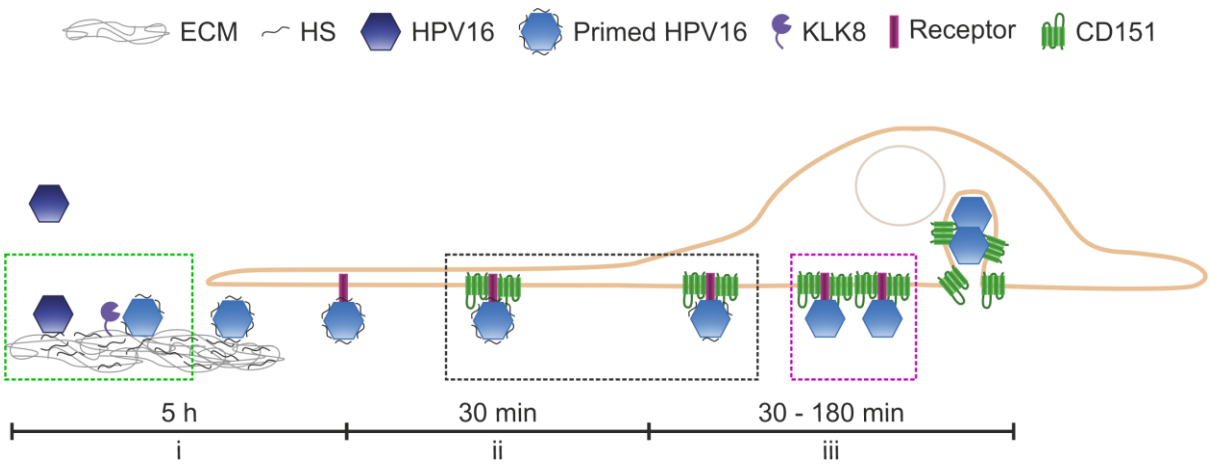

Figure 9. *Model of ECM events, actin transport, and receptor engagement in HPV16 entry.* (i) During 5 h of incubation with CytD, the PsVs bind to HS of the ECM, are primed, and become coated with HS cleavage products, enabling them for cell surface receptor engagement. (ii) After CytD removal, within 15 min, HS-decorated viruses move along filopodia to the cell body and associate with CD151 assemblies (completed within 30 min), likely located at the filopodia. (iii) Eventually, they lose their HS coat, and individual HPV16-CD151 assemblies agglomerate into larger structures (platforms), which are subsequently endocytosed. Dashed rectangles mark PsVs representing populations as defined in Figure 7. Dashed green rectangle, PsVs with a distance to HS < 250 nm and to Itgα6 > 250 nm. Dashed black rectangle, PsVs with a distance to HS < 250 nm and to Itgα6 < 250 nm. Dashed magenta rectangle, PsVs with a distance to HS > 250 nm and to Itgα6 < 250 nm.

1245 **Supplementary information**

1246

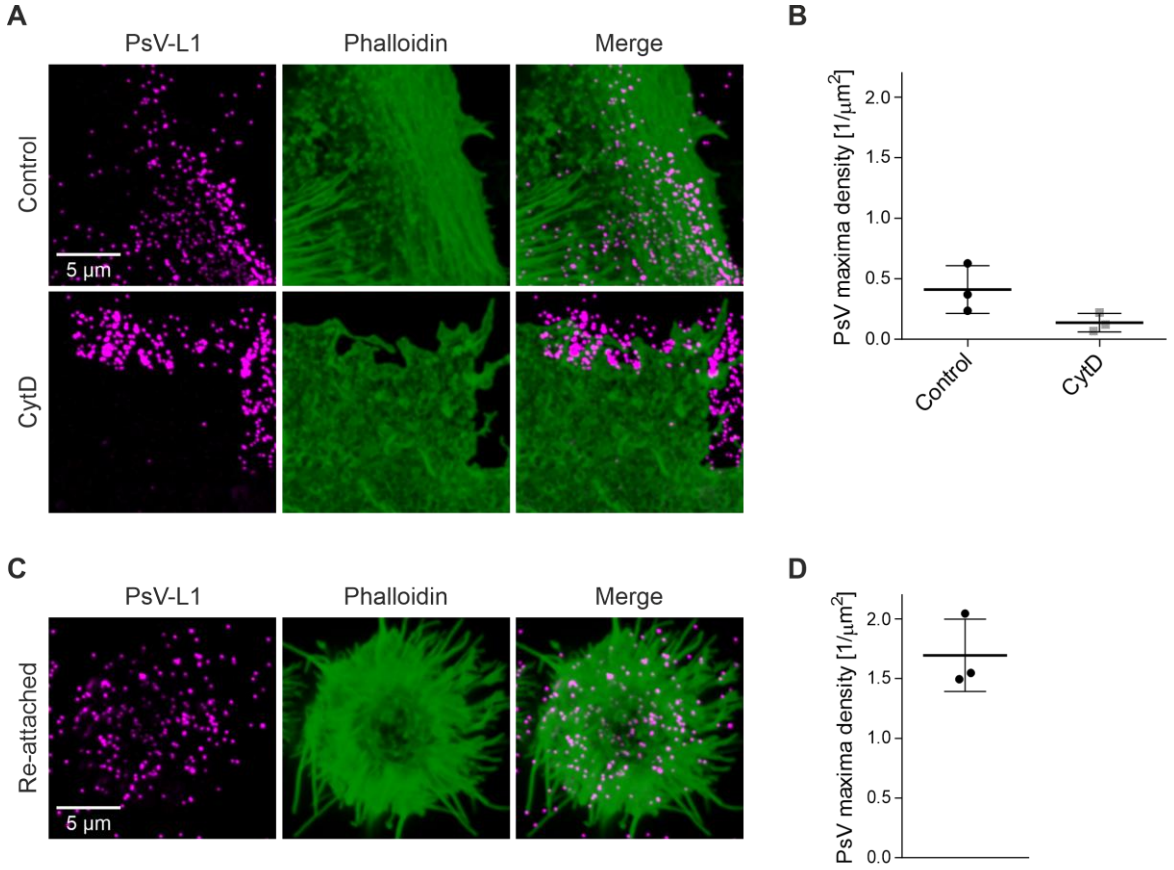

1247

1248 **Supplementary Figure 1.** *PsV density at the adhered membrane of substrate-adhered grown and re-*
1249 *attached HaCaT cells.*
1250 (A) The shown HaCaT cells are from the 0 min time point (top, Control; bottom, CytD) of the
1251 experiment described in Figure 5. Only the PsV-L1 (STAR GREEN; magenta LUT) and the F-actin
1252 phalloidin (iFluor647; green LUT) staining are shown. (B) In order to count the PsVs at the basal
1253 membrane, we placed ROIs covering only the cell body. Within these ROIs the PsV maxima were
1254 counted and related to the size of the analyzed area. Values are given as means ± SD (n = 3 biological
1255 replicates). Statistical differences between Control and CytD were analyzed by using the two-tailed,
1256 unpaired student's *t*-test (n = 3), but the analysis yielded no p-value below 0.05. (C) HaCaT cells were
1257 detached by a 15 min incubation with 10 mM EDTA (in PBS) and incubated with PsVs at 4 °C for 1 h
1258 under constant rotation. After washing the cells three times with PBS, they were seeded onto PLL-
1259 coated glass coverslips for 1 h. Then, cells were washed, fixed and stained for L1 (STAR GREEN;
1260 magenta LUT) by indirect immunofluorescence and for F-actin by iFluor647-labelled phalloidin (green
1261 LUT). PsV-L1 and F-actin staining were imaged as in (A) in the confocal mode of a STED microscope.
1262 (D) Analysis as in (B). Values are given as means ± SD (n = 3 biological replicates).

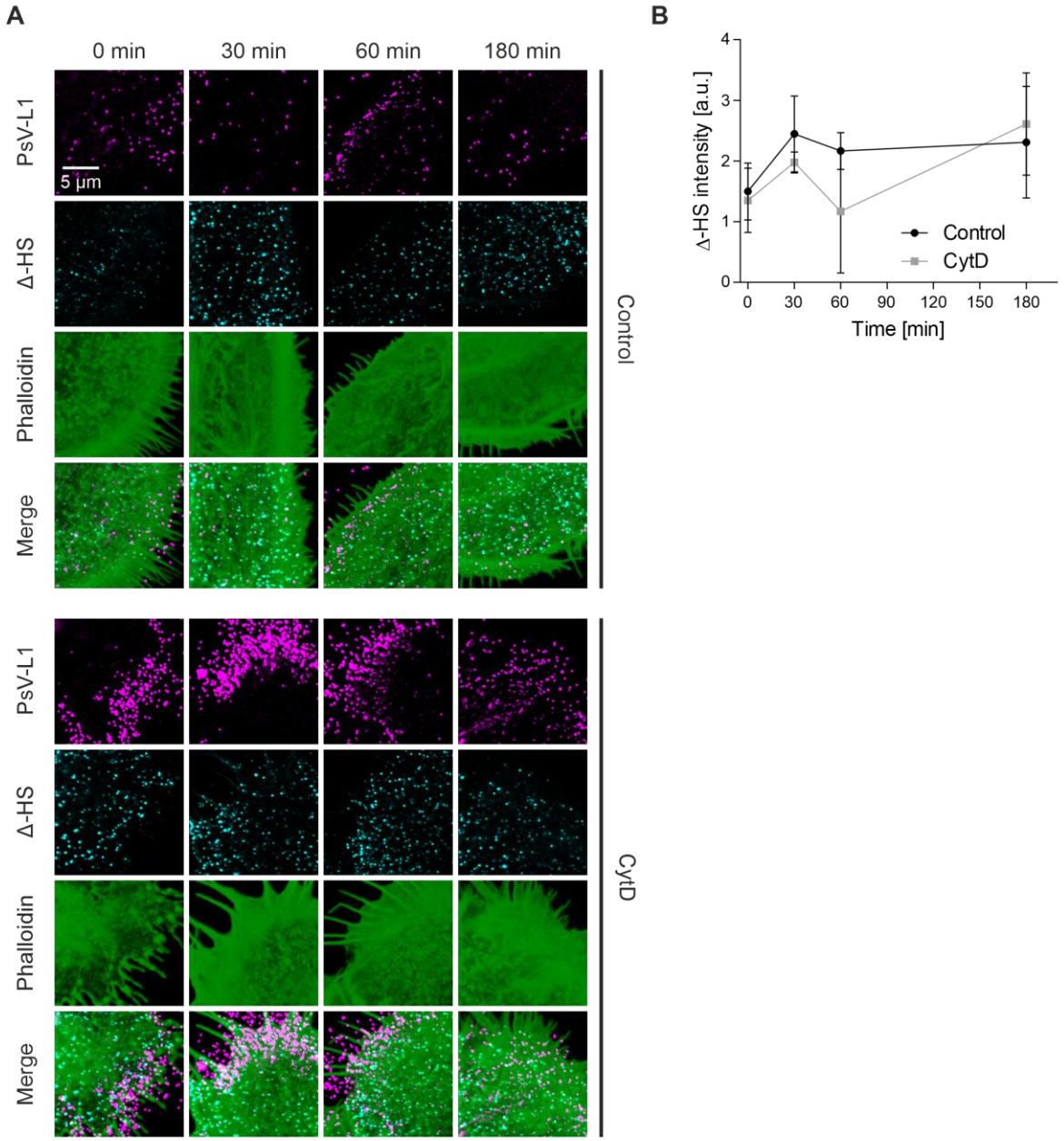

Supplementary Figure 2. *HS neo-epitope (Δ-HS) staining intensity after CytD treatment.* (A) HaCaT cells were incubated with PsVs at 37 °C for 5 h, in the absence (Control, upper panels) or presence of 10 µg/ml CytD (CytD, lower panels). Afterwards, cells were washed and incubated without PsVs/CytD further for up to 180 min, before they were fixed and stained. Immunofluorescence was used for the visualization of L1 (STAR GREEN; magenta LUT) and the HS neo-epitope, referred to as Δ-HS (AlexaFluor 594; cyan LUT). F-actin was stained by iFluor647-labelled phalloidin (green LUT). PsV-L1, Δ-HS and F-actin staining were imaged in the confocal mode of a STED microscope. For analysis, we placed large ROIs onto the images that covered mainly the cell body but included parts of the cell periphery as well. (B) The mean Δ-HS intensity over time. Values are given as means ± SD (n = 3 biological replicates). Statistical differences between the same time points of Control and CytD were analyzed by using the two-tailed, unpaired student's *t*-test (n = 3), but the analysis yielded no p-values below 0.05.

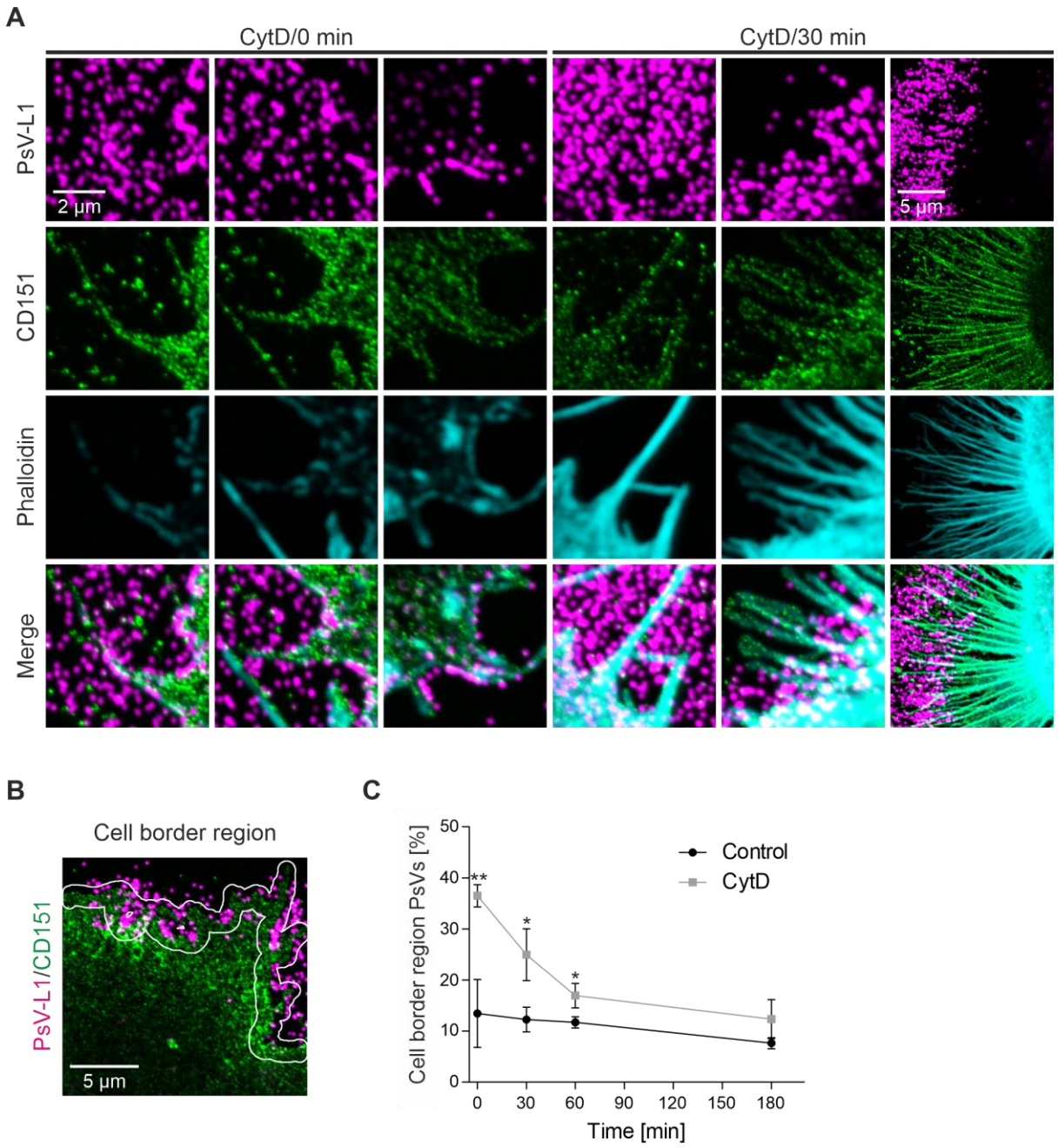

Supplementary Figure 3. *Variability of filopodia/diminishment of PsVs from the cell border region after CytD removal.*

(A) More images from the experiment described in Figure 5. We observed that many cells exhibit filopodia. Due to the large variability in number and shape we cannot show a representative image. Instead, we present for the CytD condition (0 min and 30 min) a variety of cells with CD151 positive filopodia. (B) Based on the CD151 image (green LUT), a cell border strip is defined and broadened by 20 pixels on each side, in the following referred to as the cell border region (for details see materials and methods). Please note that the cell border region is different from the cell periphery described in Figure 4 that delineates the cell body from the periphery. Instead, the cell border region covers both sides of the cell border (approximately two thirds inside and one third outside of the cell; for details see methods). (C) Diminishment of PsV maxima from the cell border region over time, expressed as percentage of all PsVs present in the image. Values are given as means ± SD (n = 3 biological replicates). Statistical differences between the same time points of Control and CytD were analyzed by using the two-tailed, unpaired student's *t*-test (n = 3, for details see materials and methods).

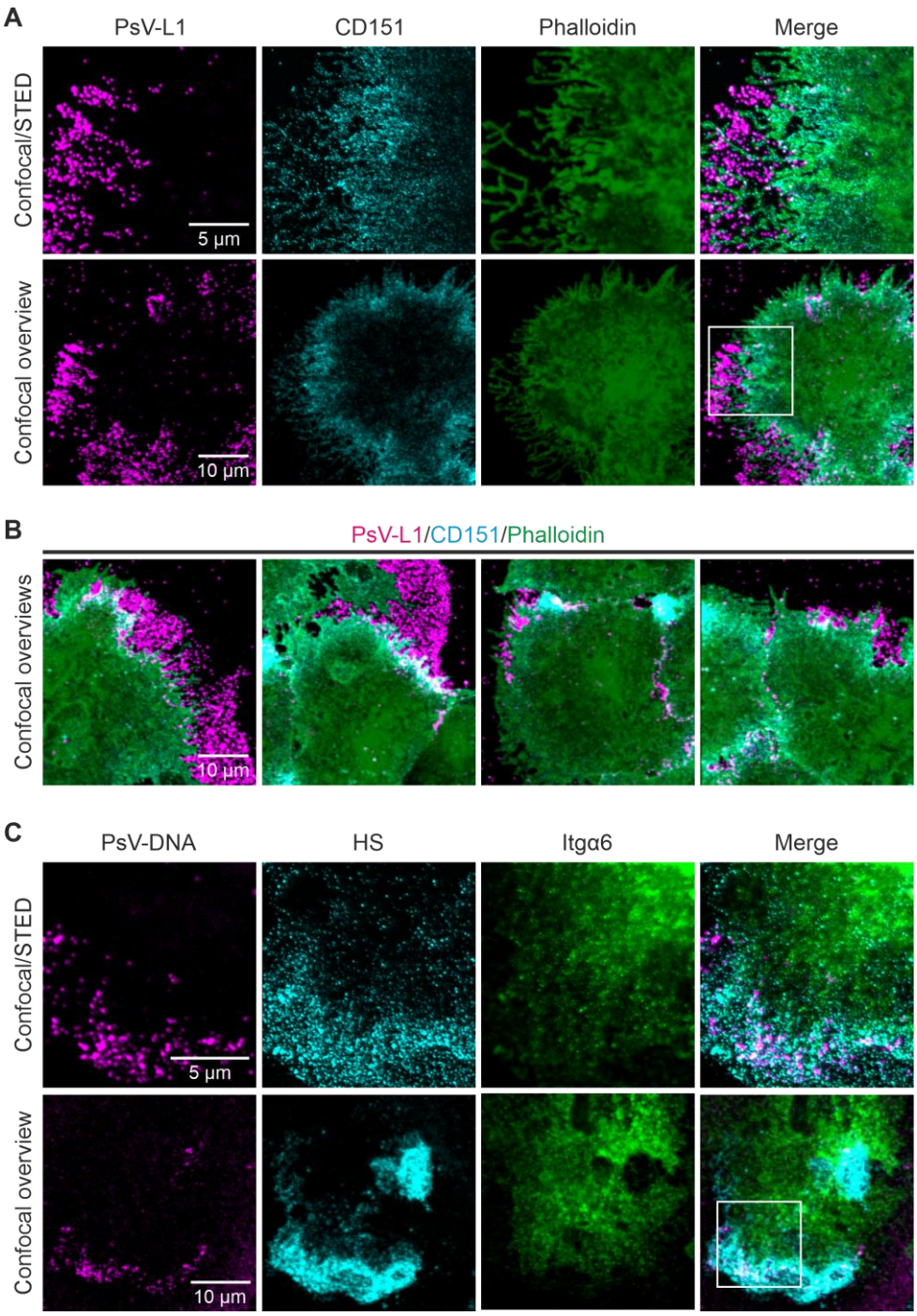

Supplementary Figure 4. *Overview images.*
(A) Upper row, micrographs from Figure 5, CytD/0min, showing as well F-actin staining (green LUT) and CD151 using the cyan LUT. Lower row, confocal overview. After taking the overview, the area in the white box was imaged as described in the legend of Figure 5, yielding the images shown in the upper row in A. (B) More overview images from the experiment described in Figure 5, condition CytD/0 min, showing examples of large and small PsV accumulations. (C) Upper row, micrographs from Figure 6, CytD/0 min. Lower row, confocal overview. The area in the white box was imaged as described in the legend of Figure 6, yielding the images of the upper row in C.

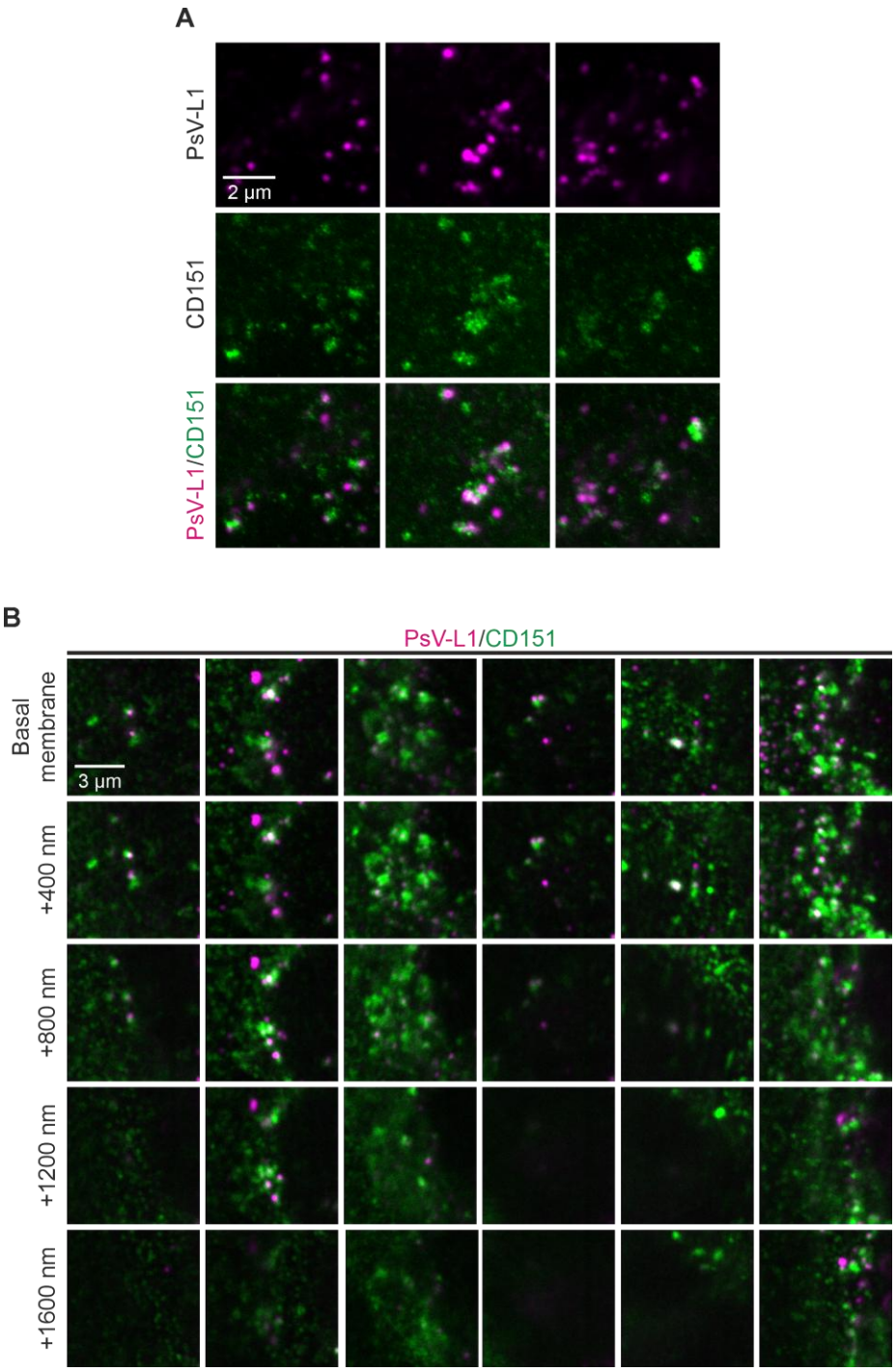

1302

1303 **Supplementary Figure 5.** *Examples of agglomerated CD151 maxima associated with PsVs that*
1304 *presumably represent endocytic structures.*
1305 (A) From the CytD/180 min time point described in Figure 5, we show more examples of agglomerated
1306 CD151 maxima (green LUT, see green patches) that associate with PsVs (magenta LUT). (B) Same
1307 experiment as in (A). Starting at the basal membrane, at confocal resolution we imaged CD151 (green
1308 LUT) and PsV-L1 (magenta LUT). Cells were further scanned by 400 nm steps in the axial direction.
1309 Some of the CD151 agglomerates noticed in the basal membranes appear to continue deeper into the
1310 cell, more than a micrometer in the second example from the left. We propose that the agglomerated
1311 CD151 maxima close to PsVs feature the characteristics of endocytic structures, as CD151 has been
1312 shown to co-internalize with PsVs (***Scheffer et al., 2013***), and as these structures invaginate into the
1313 cell, like PsV filled tubular organelles previously described by electron microscopy (***Schelhaas et al.,***

1314 ***2012***). Images in (A) and (B) are shown at the same settings of brightness and contrast but at different
1315 settings compared to Figure 5.
1316

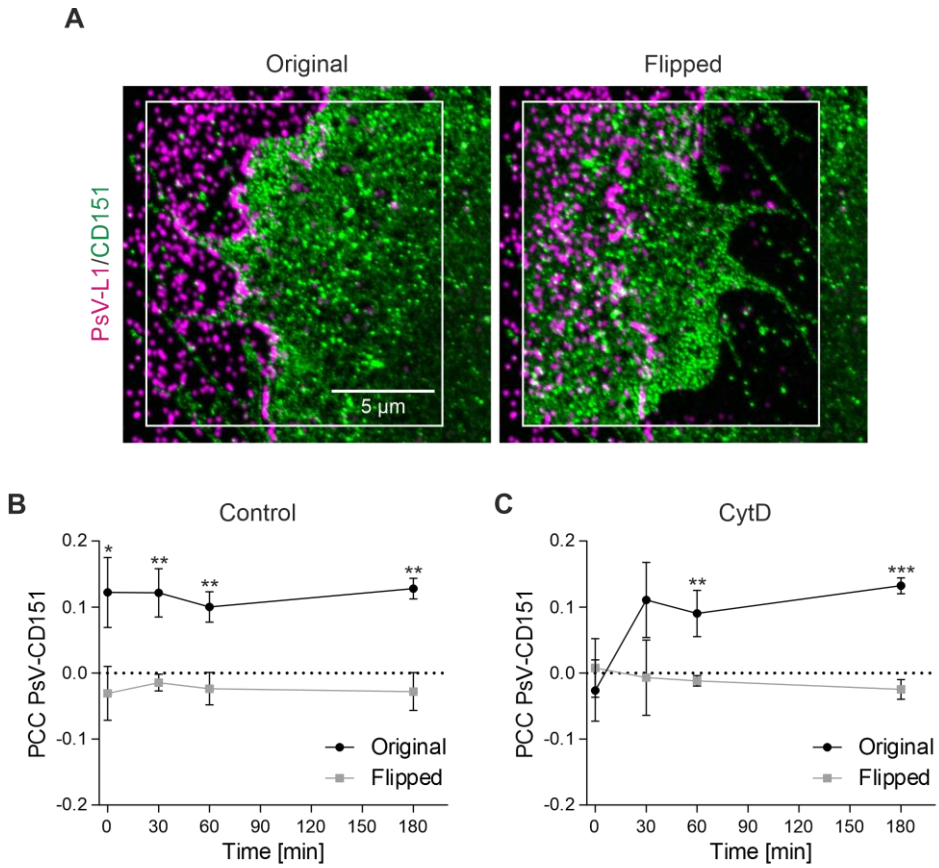

Supplementary Figure 6. *PCC values of flipped images.*
(A) For each image pair, we determined the PCC on respective non-overlapping images that have the same density of objects and intensities. To this end, one channel was flipped horizontally and vertically. Left, original images (from the CytD/0 min condition). The ROI for analysis is illustrated as white box. Right, in the ROI, the CD151 image (green LUT) was flipped horizontally and vertically. (B + C) Shown are the PCCs over time of Figure 5C obtained on the original images ((B) Control, (C) CytD) together with the PCCs of the flipped images. Values are given as means ± SD (n = 3 biological replicates). Statistical differences between the same time points of original and flipped images was analyzed by using the two-tailed, unpaired student's *t*-test (n = 3, for details see methods).

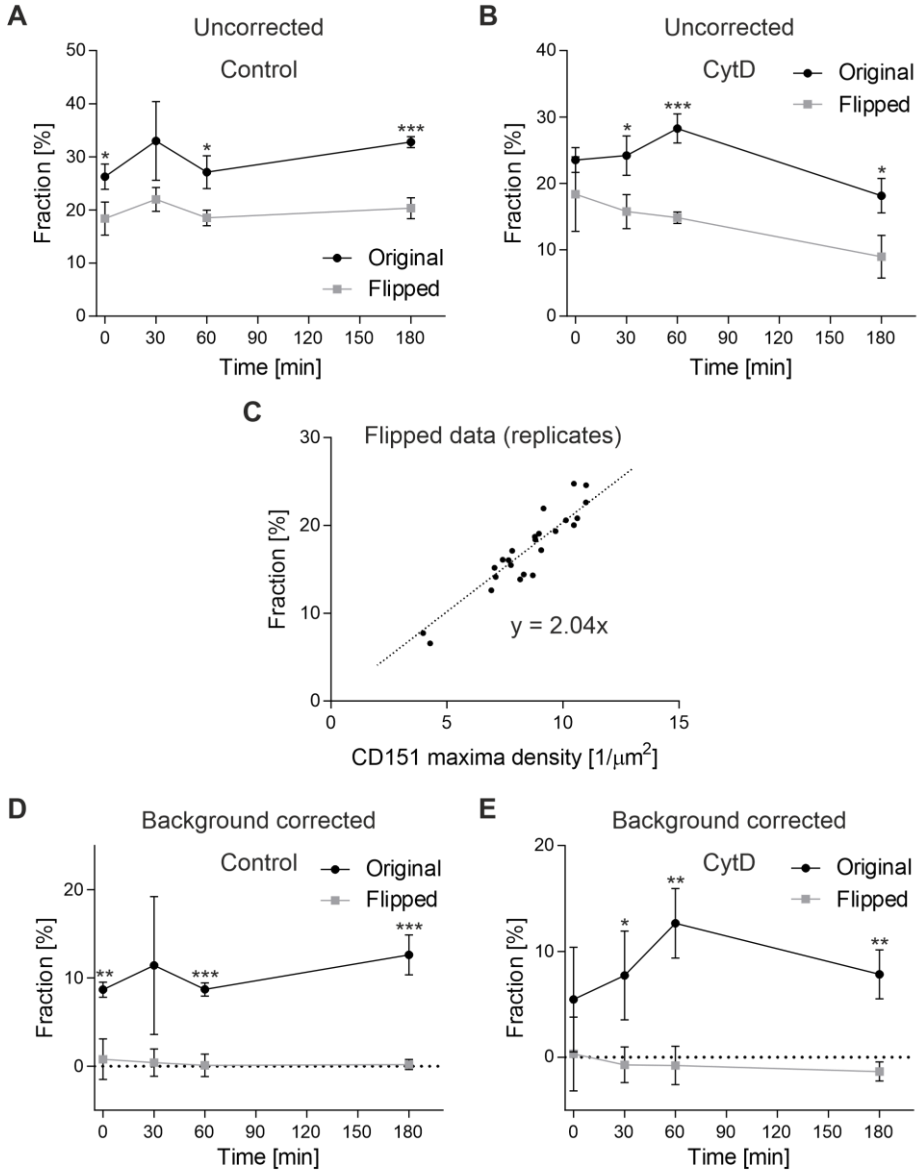

Supplementary Figure 7. *Background correction of the fraction of PsVs closely associated with CD151.* (A) The fraction of closely associated PsVs (PsV-L1 maxima with a distance ≤ 80 nm to the next nearest CD151 maximum) in the Control of Figure 5 was analyzed on original and flipped images (for an example of a flipped image see Supplementary Figure 6A). On flipped images, we often find values more than half of the values of the original images, demonstrating that many PsVs have a distance ≤ 80 nm to CD151 merely by chance (background association). (B) Same as (A), for CytD. (C) Each time point in (A) and (B) obtained from flipped images is the average of three biological replicates. We use these altogether 24 data points, plotting the fraction of closely associated PsVs against the CD151 maxima density. The fraction increases with the maxima density, as the chance of random association increases with the maxima density. The fitted linear regression line describes the dependence of the background association from the maxima density. As a result, the background association (y) can be calculated for any maxima density (x) in original images with the equation y = 2.04x. Please note that the CytD/0 min may be overcorrected as we subtract background association with reference to the CD151 maxima density of the entire ROI (for an example ROI see Supplementary Figure 6A), although the local maxima density at distal PsVs is lower. On the other hand, PsVs at the cell border may have a larger local CD151 maxima density and consequently are undercorrected. (D) and (E), for each original and flipped image of (A) and (B), the background was calculated and subtracted from the uncorrected value. The original background corrected values in (D) and (E) are shown in Figure 5D.

1346 Values are given as means ± SD (n = 3 biological replicates). Statistical differences between the same
1347 time points of original and flipped images were analyzed by using the two-tailed, unpaired student's *t*-
1348 test (n = 3, for details see methods).
1349

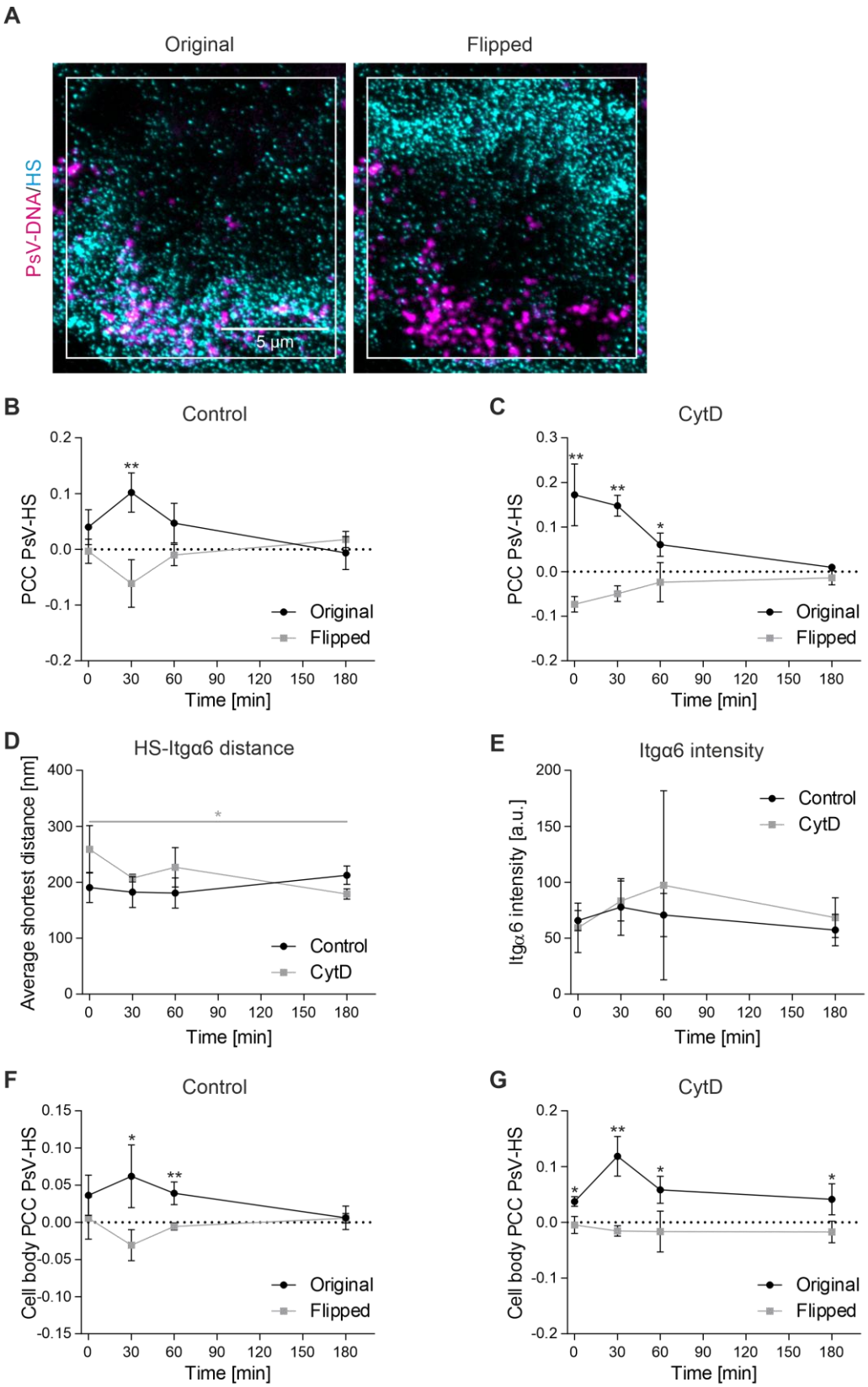

Supplementary Figure 8. *PCC values of flipped images, HS-Itgα6 shortest distance and Itgα6 intensity.* (A) For each image pair, we determined the PCC on respective non-overlapping images that have the same density of objects and intensities. To this end, one channel was flipped horizontally and vertically. Left, original images (from the CytD/0 min condition). The ROI for analysis is illustrated as white box. Right, in the ROI, the HS image (cyan LUT) was flipped horizontally and vertically. (B + C)

1356 Shown are the PCCs over time of Figure 6C obtained with the original images ((B) Control, (C) CytD)
1357 together with the PCCs of the flipped images. (D) The shortest distance of HS maxima to the next
1358 nearest Itgα6 maxima over time. (E) The mean Itgα6 intensity over time. (F + G) Shown are the PCCs
1359 over time of Figure 6D obtained with the original images ((F) Control, (G) CytD) together with the PCCs
1360 of the flipped images. Values are given as means ± SD (n = 3 biological replicates). Statistical
1361 differences between the same time points of original and flipped images ((B), (C), (F) and (G)) or
1362 Control and CytD (E). (D) Difference between CytD/0 min and CytD/180 min. Statistical differences
1363 were analyzed by using the two-tailed, unpaired student's *t*-test (n = 3, for details see methods).
1364

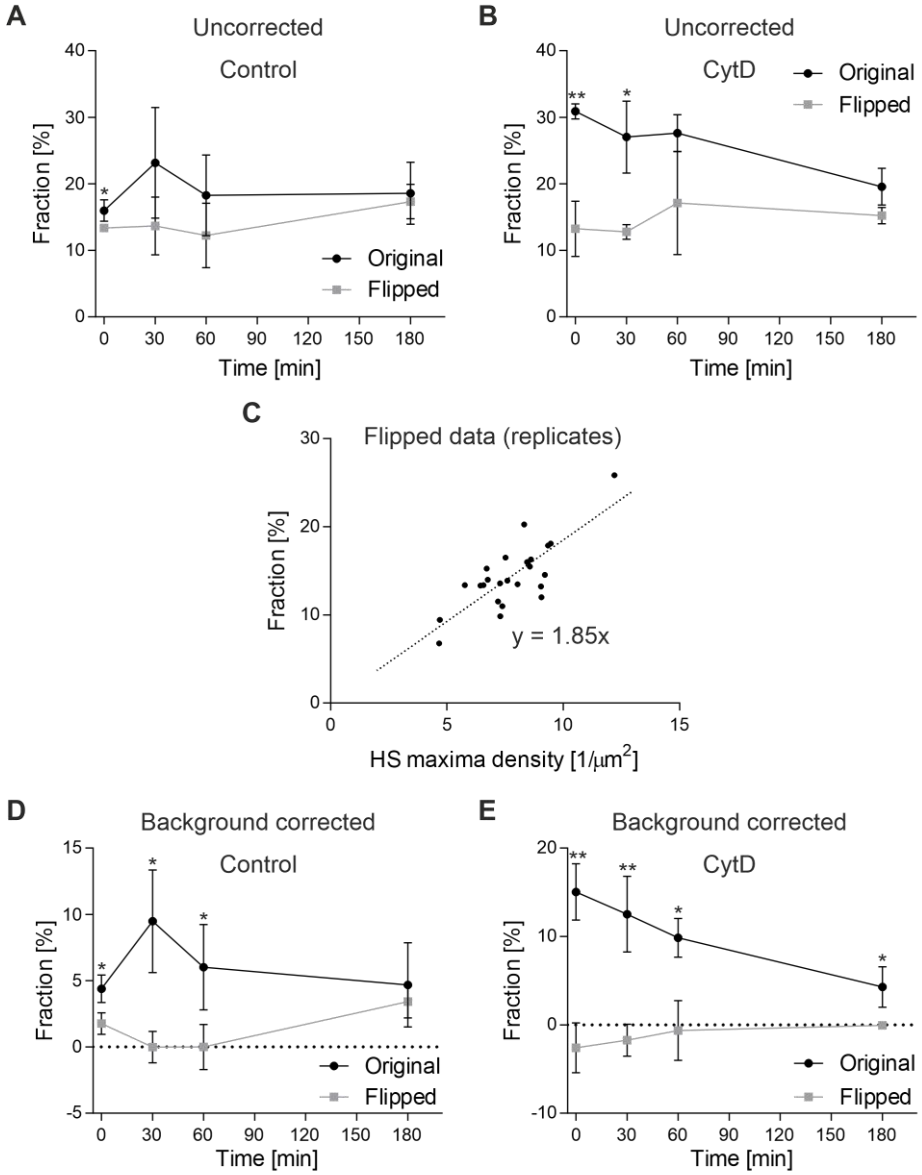

Supplementary Figure 9. *Background correction of the fraction of PsVs closely associated with HS.* (A) The fraction of closely associated PsVs (PsV-DNA maxima with a distance ≤ 80 nm to the next nearest HS maximum) in the Control of Figure 6 was analyzed on original and flipped images (for an example of a flipped image see Supplementary Figure 8A). (B) Same as (A), for CytD. (C) From the altogether 24 analyzed flipped images, we obtained the equation y = 1.85x for calculating the background association (please see Supplementary Figure 7 for more details). (D) and (E), background corrected graphs of (A) and (B). For each original and flipped image the background was calculated and subtracted from the uncorrected value. The original background corrected values in (D) and (E) are shown in Figure 6E. Values are given as means ± SD (n = 3 biological replicates). Statistical differences between the same time points of original and flipped images were analyzed by using the two-tailed, unpaired student's *t*-test (n = 3, for details see methods).

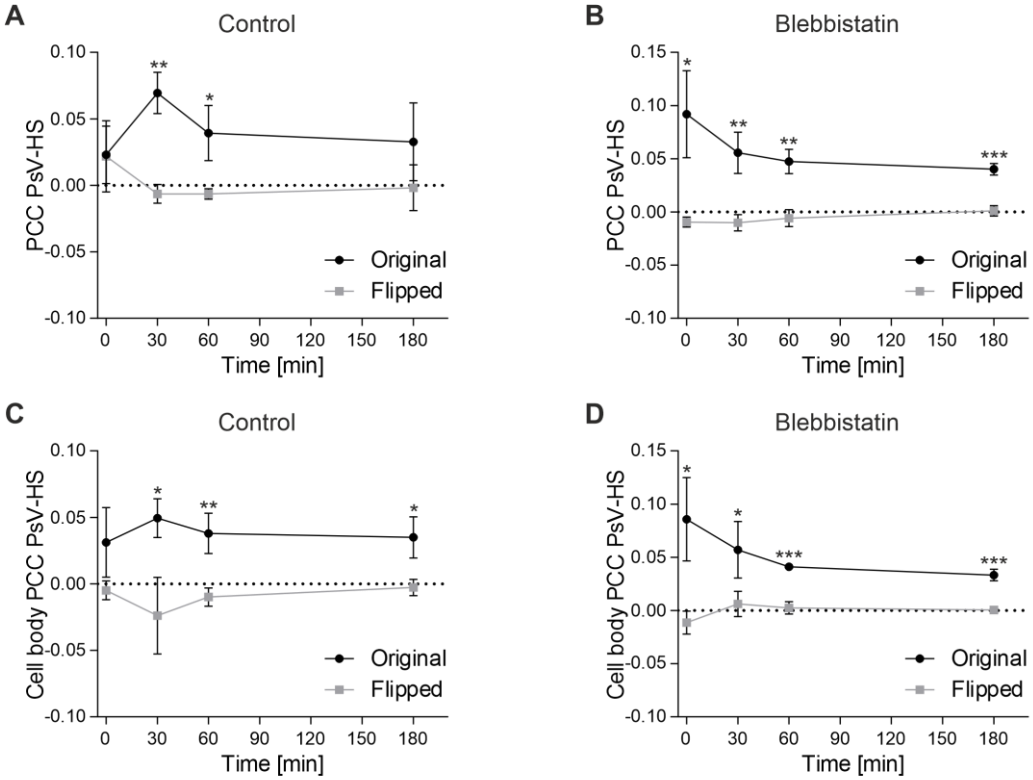

Supplementary Figure 10. *PCC values of flipped images.*
(A) and (B) The PCC values between PsV and HS of Figure 8C ((A) Control, (B) Blebbistatin) plotted together with the respective PCC values of flipped images. (C) and (D) The cell body PCC values between PsV and HS of Figure 8D ((C) Control, (D) Blebbistatin) plotted together with the respective PCC values of flipped images. Values are given as means ± SD (n = 3 biological replicates). Statistical differences between the same time points of original and flipped images were analyzed using the two-tailed, unpaired student's *t*-test (n = 3, for details see methods).

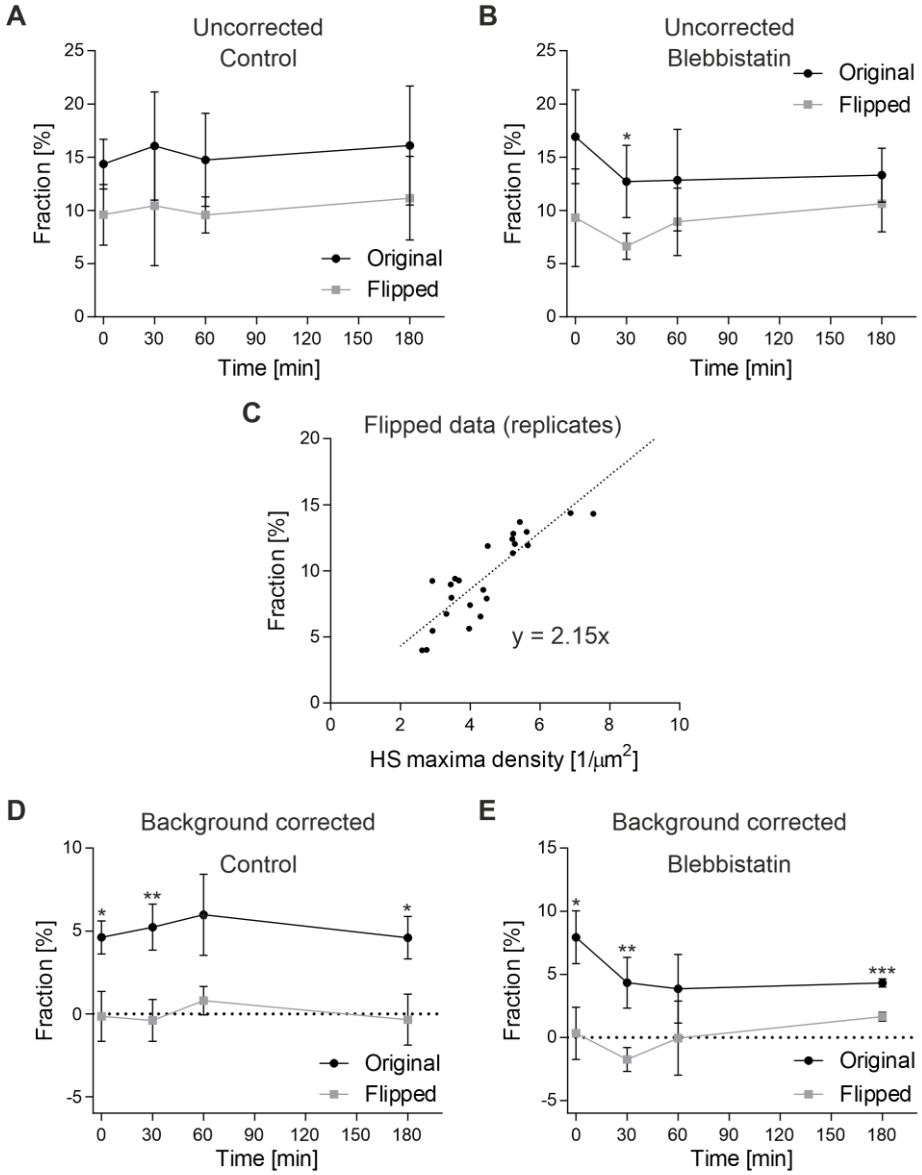

Supplementary Figure 11. *Background correction of the fraction of PsVs closely associated with HS upon blebbistatin treatment.*

(A) The fraction of closely associated PsVs (PsV-L1 maxima with a distance ≤ 80 nm to the next nearest HS maximum) in the Control of Figure 8 was analyzed on original and flipped images. (B) Same as (A), for blebbistatin. (C) From the altogether 24 analyzed flipped images, we obtained the equation y = 2.15x for calculating the background association (please see Supplementary Figure 7 for more details). (D) and (E), background corrected graphs of (A) and (B). For each original and flipped image the background was calculated and subtracted from the uncorrected value. The original background corrected values in (D) and (E) are shown in Figure 8E. Values are given as means ± SD (n = 3 biological replicates). Statistical differences between the same time points of original and flipped images were analyzed by using the two-tailed, unpaired student's *t*-test (n = 3, for details see methods).

Supplementary Table 1. Fraction of PsVs in percent of each of the four distance categories (see left column). Values are means ± SD of the data shown in Figure 7B. For each time point and category, p-values between Control and CytD were calculated by using the two-tailed, unpaired student's *t*-test (n = 3 biological replicates). P-values < 0.05 are illustrated in bold.

	0 min			**30 min**			**60 min**			**180 min**		
	Control [%]	CytD [%]	p-value	Control [%]	CytD [%]	p-value	Control [%]	CytD [%]	p-value	Control [%]	CytD [%]	p-value
HS < 250 nm & Itgα6 < 250 nm	62.31 ± 5.05	47.83 ±3.26	**0.0271**	65.48 ± 8.35	63.67 ± 1.14	0.7764	59.06 ± 10.64	67.16 ± 9.84	0.4739	63.69 ± 4.27	59.28 ± 3.17	0.3065
HS < 250 nm & Itgα6 > 250 nm	12.18 ± 5.51	46.04 ± 3.67	**0.0019**	15.46 ± 3.14	26.12 ± 2.16	**0.0167**	13.25 ± 1.94	19.87 ± 3.12	0.0637	11.97 ± 1.53	10.64 ± 1.15	0.3808
HS > 250 nm & Itgα6 < 250 nm	21.59 ± 4.07	4.34 ± 0.37	**0.0040**	15.83 ± 5.73	8.58 ± 2.33	0.1723	23.49 ± 6.55	9.60 ± 4.81	0.0731	20.88 ± 3.31	25.24 ± 1.96	0.1842
HS > 250 nm & Itgα6 > 250 nm	3.93 ± 0.30	1.79 ± 0.60	**0.0110**	3.23 ± 0.88	1.63 ± 0.21	0.0675	4.19 ± 2.43	3.38 ± 2.20	0.7425	3.46 ± 0.54	4.84 ± 2.87	0.5393